MEASUREMENTS OF PLASMA, PLASMA WAVES, AND SUPRATHERMAL CHARGED PARTICLES IN SATURN'S INNER MAGNETOSPHERE

F. L. SCARF
TRW Space and Technology Group

L. A. FRANK, D. A. GURNETT
University of Iowa

L. J. LANZEROTTI
Bell Laboratories

A. LAZARUS
Massachusetts Institute of Technology

and

E. C. SITTLER, JR.
NASA Goddard Space Flight Center

The Pioneer 11 and Voyager 1, 2 traversals of Saturn's inner magnetosphere provided direct information on the complex and highly structured distributions of plasma and suprathermal charged particles present in this region. The Voyager wave instruments also yielded absolute electron density measurements in certain inner magnetosphere locations; the wave data were used to evaluate the magnitudes of several wave-particle interactions. We summarize the plasma and wave measurements for 24-hr periods centered around closest approach, evaluate pitch-angle scattering effects possibly associated with measured

whistler mode turbulence, and speculate on the effects of wave-particle interactions associated with electrostatic waves.

Within a two-year period extending from September 1979 to August 1981 Saturn was visited by three spacecraft: Pioneer 11, Voyager 1, and Voyager 2. During short intervals associated with each encounter, the three spacecraft transmitted back to Earth local measurements that provide us with essentially all that is now known about the structure and dynamics of Saturn's magnetosphere. Some supplementary magnetospheric information of significance was obtained during the two Voyager approaches to the planet as the planetary radio astronomy investigations measured detailed characteristics of escaping Saturn radio emissions. However, these Saturn emissions are of such low intensity that remote sensing from Earth or from Earth orbit yields no magnetospheric information at all. Thus, the spacecraft *in situ* measurements from Pioneer and Voyager are of particular scientific importance.

While the Pioneer and Voyager encounters with Saturn supplied a wealth of definitive new knowledge, they have also introduced many fundamental questions that are still unanswered. On the positive side, we note that the Pioneer and Voyager instruments found a planetary magnetic field aligned with the planet's spin axis, an extended high-density plasma sheet, a hot ($\sim$ 35 keV) plasma in the outer magnetosphere, and a population of trapped energetic particles which interacts strongly with the inner satellites and the rings. It was determined that Titan has no intrinsic magnetic field and that this satellite is generally a significant source of plasma ions for the outer magnetosphere. It was also determined that the vast hydrogen torus extending from $\sim$ 8 to 25 R_S plays an important role as a source of plasma and as a medium interacting with ions which originate in other source regions. However, the relative importance of other plasma sources (such as the solar wind, the Saturn atmosphere, the ice-covered surfaces of the inner satellites and the rings) has not been conclusively established.

Since present understanding of the sources and sinks of plasma and suprathermal charged particles in Saturn's magnetosphere is highly incomplete, we concentrate here on measurement descriptions. Attention is focused on plasma physics problems in the inner magnetosphere, which we define as the region traversed during each 24-hr period centered around closest approach. In complementary reports, Schardt et al. discuss Saturn's outer magnetosphere ($L > 10$), Van Allen concentrates on the interactions of energetic charged particles with Saturn's rings and satellites, Connerney et al. describe Saturn magnetic-field models, and Kaiser et al. discuss Saturn radio emissions (see their respective chapters in this book). None of these topics are treated in detail here; the emphasis on questions of plasma physics at Saturn naturally leads to a strong focus on the Voyager observations since Pioneer 11 had no instruments to measure suprathermal charged particles or the characteristics of plasma waves.

I. PIONEER 11, VOYAGER 1 AND 2 TRAJECTORIES

All three spacecraft approached Saturn near the noon meridian. Both Voyager 2 and Pioneer 11 left the magnetosphere of Saturn near the dawn meridian, while Voyager 1 exited further down the tail at a local time of 0400.

Figure 1 gives information about the radial and latitudinal coverage of Saturn's magnetosphere by the three spacecraft. In each case the trajectory segment shown covers the 24-hr period centered about closest approach. The trajectories in Fig. 1 are given in a cylindrical Saturn-centered coordinate system, the Z axis is aligned along Saturn's spin axis, and R is the equatorial radial distance from Saturn. The lack of a tilt and offset for the planetary magnetic field makes the spin equator nearly congruent with the magnetic equator. While this makes modeling studies easier, it also has the unfortunate consequence that each spacecraft, during an encounter interval, does not make as many crossings of Saturn's plasma sheet as was the case during the Jupiter encounters (see Scarf et al. 1983, for further discussion of this point). The symmetry introduced by Saturn's internal magnetic field also makes the centrifugal and magnetic equatorial planes nearly coincident. Under this condition, the plasma, regardless of its thermal characteristics, will have mirror symmetry about the equatorial plane.

II. PLASMA OBSERVATIONS

Although the plasma probe on Pioneer 11 was designed for solar wind observations, this instrument was able to measure characteristics of magnetospheric ions within the energy-per-unit charge E/Q range of 100 eV to 8 keV on the inbound pass between $\sim$ 16 R_S and 4 R_S (Wolfe et al. 1980; Frank et al. 1980). In the inner magnetosphere ($\leq$ 10 R_S), the ions were found to be rigidly corotating with the planet, and at radial distances beyond the orbit of Rhea (8.8 R_S), these ions were identified as protons with typical average densities and temperatures near 0.5 cm^{-3} and 10^6 K, respectively. In some regions, the mass-per-unit charge M/Q of the dominant ions could also be determined by analysis of the angular distributions. Figure 2 shows Pioneer 11 profiles of the ion density and ion temperature adopted from the report by Frank et al. (1980); the ion composition identifications are also marked here.

Frank et al. concluded that a large torus of oxygen ions is located inside the orbit of Rhea, with densities $\gtrsim$ 10 cm^{-3} over the radial distance range of $\sim$ 4 R_S to 7.5 R_S. They noted that density maxima appear at the orbits of Dione and Tethys where oxygen ion densities are $\sim$ 50 cm^{-3}. The dominant oxygen charge states were thought to be O^{2+} and O^{3+} in the radial distance ranges of $\sim$ 4 R_S to 7 R_S and 7 R_S to 8 R_S, respectively. The observations suggest a decrease of ion energies to values less than the instrument energy threshold of E/Q = 100 eV at the apparent inward edge of the torus at 4 R_S. Measured ion temperatures increased rapidly from $\sim$ 2 $\times$ 10^5 K at 4 R_S to

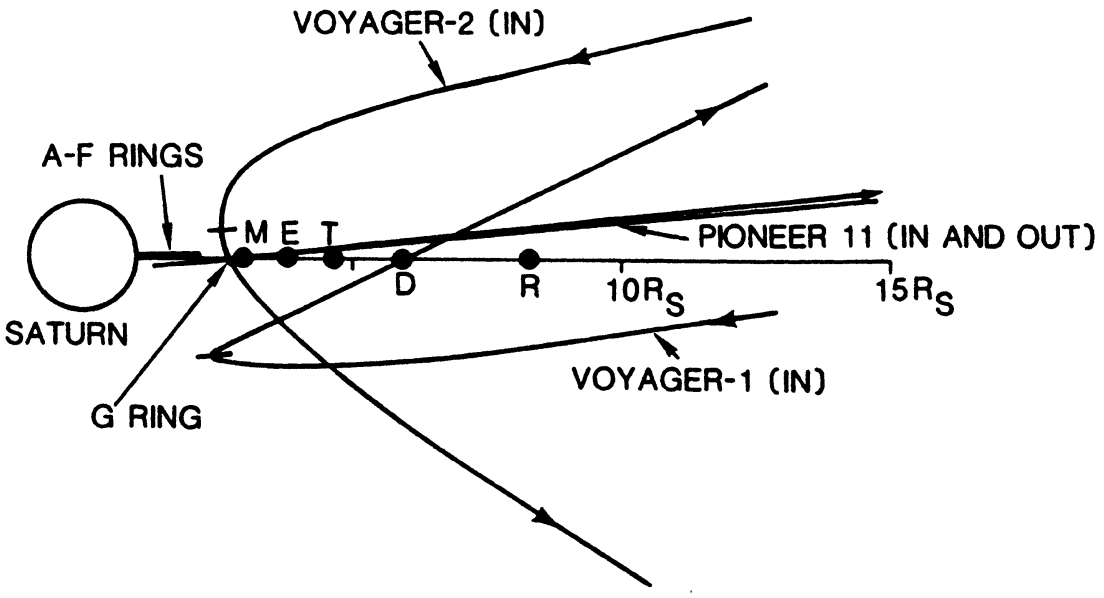

Fig. 1. Radius versus latitude trajectory plots for the Pioneer 11, Voyager 1, and Voyager 2 traversals of Saturn's inner magnetosphere. Each segment goes from 12 hr before closest approach to 12 hr beyond this point. The labels *M*, *E*, *T*, *D*, and *R* refer to the satellites Mimas, Enceladus, Tethys, Dione, and Rhea.

5×10^6 K at 7.3 R_S; it was conjectured that the most likely source of these plasmas is the photodissociation of water frost on the surface of the ring material along with ionization of the products and their subsequent outward radial diffusion.

The Voyager observations greatly extended our knowledge of plasma distributions in Saturn's magnetosphere. As shown in Fig. 1, the Voyager encounters yielded high-latitude information that was needed to estimate the thickness of the plasma sheet. In addition, the plasma probe on each spacecraft provided simultaneous high-resolution measurements of electrons and ions over an extended energy/charge range ($E/Q \approx 10$ V to 6 kV for both species), together with improved information on angular distributions. In a pair of initial reports (Bridge et al. 1981*a*,1982), the plasma probe measurements of Voyager were combined with Pioneer 11 observations to define the complex configuration of plasma in Saturn's magnetosphere. Bridge et al. (1981*a*,1982) discussed evidence for azimuthal flow of the plasma within $L = 15$, and they noted that the results were consistent with the magnetic-field rotation rate implied by Voyager radio observations (Kaiser et al. 1980). It was suggested that the ions were H^+ and O^+ (or N^+), although final identification was reserved for a later study. Three basic features in the plasma morphology were identified in these preliminary studies:

1. Highly variable regime outside $L = 15$, where abrupt changes in the plasma density by nearly an order of magnitude in < 96 s were observed;

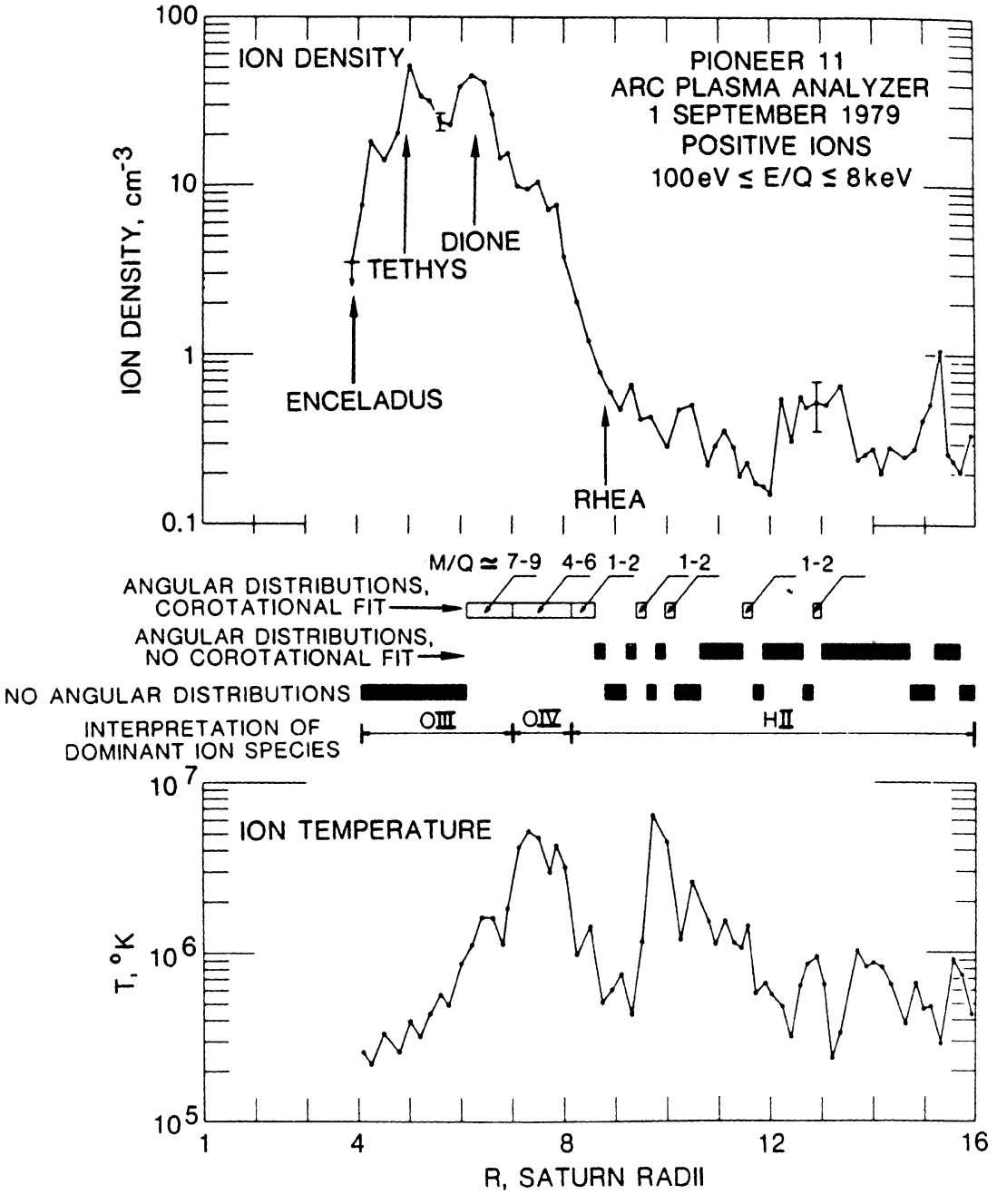

Fig. 2. Pioneer 11 ion densities, temperatures, and composition as functions of radial distance. The oxygen torus extends from ~ 4 R_S to 8 R_S. The rapid decline of densities at ~ 4 R_S may be due to ion energies decreasing with decreasing radial distance to values below the energy (E/Q) threshold of the plasma instrument at 100 eV-per-unit charge. Ion temperatures within the plasma torus at R_S to 7 R_S monotonically decrease with decreasing radial distance.

2. Extended plasma sheet between $L = 7$ and $L = 15$ with a half-thickness in the Z direction greater than 4 R_S;
3. Inner plasma torus inside $L = 7$ with a half-thickness in Z of 1 R_S at $L = 5$ and 0.2 R_S at $L = 2.88$.

A definite reduction in density scale height with decreasing L was observed; this was attributed to a reduction in plasma temperature with decreasing L and possibly a change in the pitch-angle distribution. Bridge et al. (1981*a*,1982) also estimated the total plasma content in the extended plasma sheet to exceed that in the inner plasma torus, which would rule out the inner plasma torus as the primary source for the extended plasma sheet. As noted in Sittler et al. (1983), it is premature at this time to make any conclusive comments about plasma sources until detailed scale height model calculations using both ion and electron measurements are performed.

Bridge et al. (1981*a*,1982) presented 15-min averages of the electron densities and used these data plots to discuss the configuration of Saturn's plasma sheet. Recently, Sittler et al. (1983) completed a more detailed analysis of the electron measurements. Figure 3 contains unaveraged plots of Voyager 1 and 2 electron density profiles, along with electron temperature profiles. In this figure all the principal features discussed by Bridge et al. can readily be discerned. For Voyager 1, the two broad regions of density enhancement (17 R_S to $\sim$ 7 R_S inbound; 3 R_S to 11 R_S outbound) suggest an equatorially confined plasma sheet surrounding Saturn. For the Voyager 2 pass, the corresponding density enhancements were found between 11 and 4 R_S inbound and between 4 and 16 R_S outbound.

Bridge et al. (1982) used these density profiles to construct empirical electron density models with simple functional forms such as $n_e L^4 \approx 5.5 \times 10^3$ cm^2 in the extended plasma sheet ($L \approx 8.5$ to 15) and $n_e L^3 \approx 2.4 \times 10^3$ cm^2 in the inner plasma sheet ($L \approx 4$ to 7.5). They showed that these models provided reasonable fits to most of the observations from Pioneer 11 (Fig. 2) and from both Voyagers (Fig. 3). This result suggests a reasonably stable spatial configuration for the Saturn plasma sheet, of the form sketched in Fig. 4.

An extremely interesting characteristic of Saturn's plasma is that the magnetospheric electrons have spectra with distinct hot (suprathermal) and cold (thermal) components. Figure 5 shows electron speed distributions measured near the Voyager 1 outbound ring-plane crossing. The dashed lines indicate Maxwellian fits to the cold component; the hot density n_H and hot temperature T_H were computed by setting $n_H = n_e - n_c$ and $T_H = (n_e T_e - n_c T_c)/n_H$. More examples are contained in the report by Sittler et al. (1983).

The Voyager electron measurements display large-scale radial gradients in electron temperature with T_e increasing from < 1 eV in the inner magnetosphere to as high as 800 eV in the outer magnetosphere. This increase in

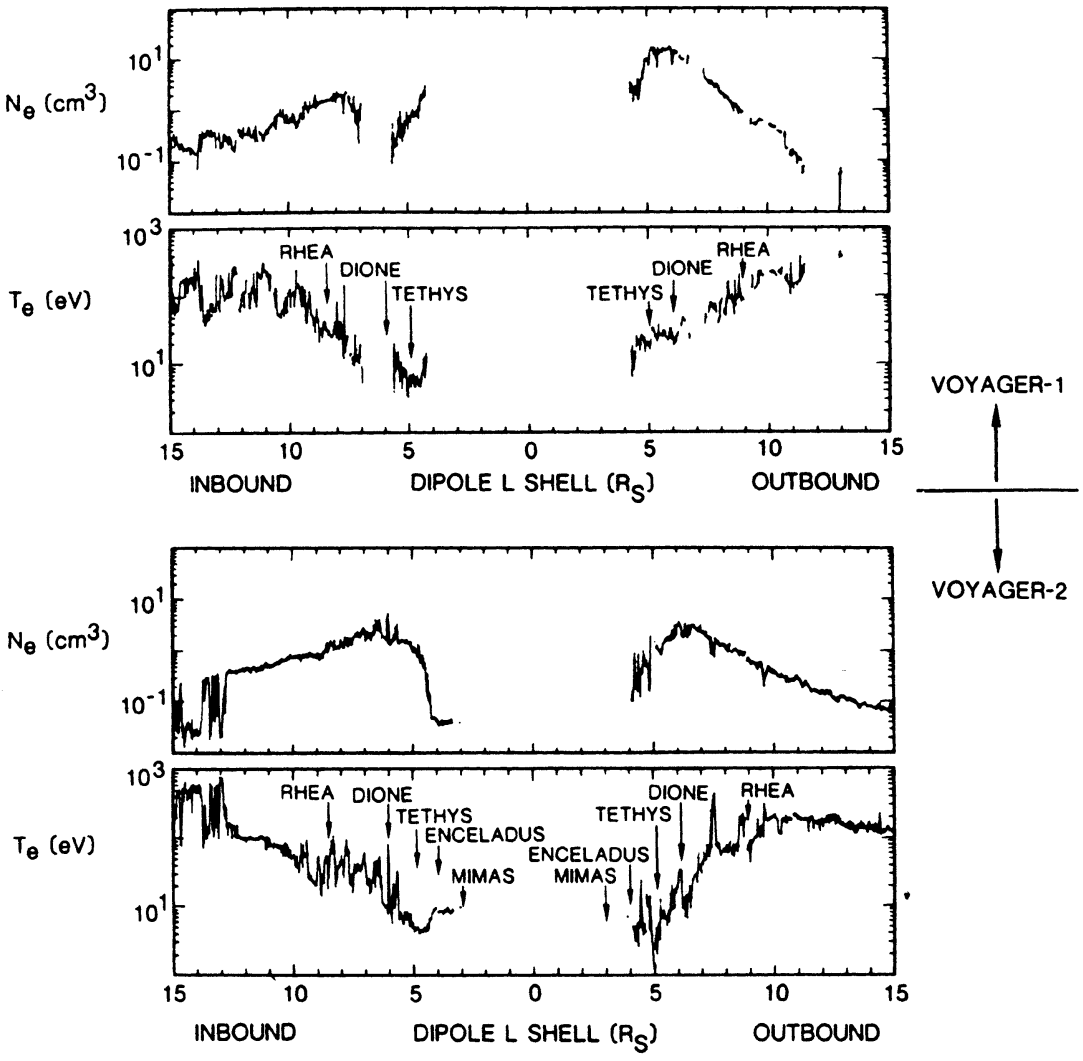

Fig. 3. Electron density and temperature profiles derived from observations of Voyagers 1 (top) and 2 (bottom) plasma probe (Sittler et al. 1983).

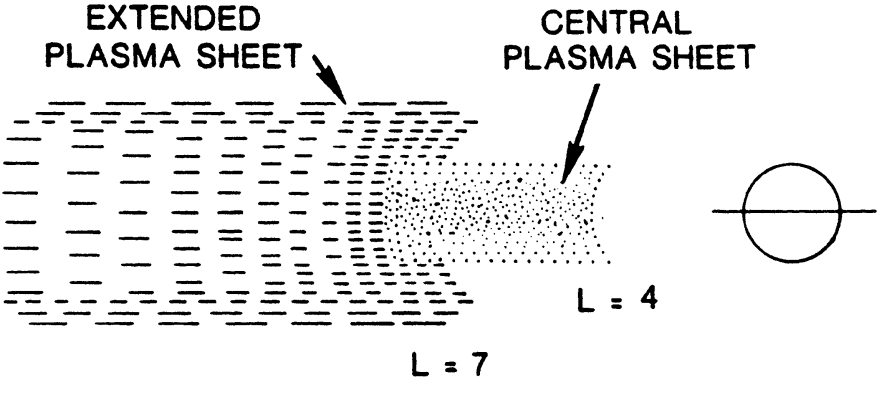

Fig. 4. Possible configuration of Saturn's plasma sheet.

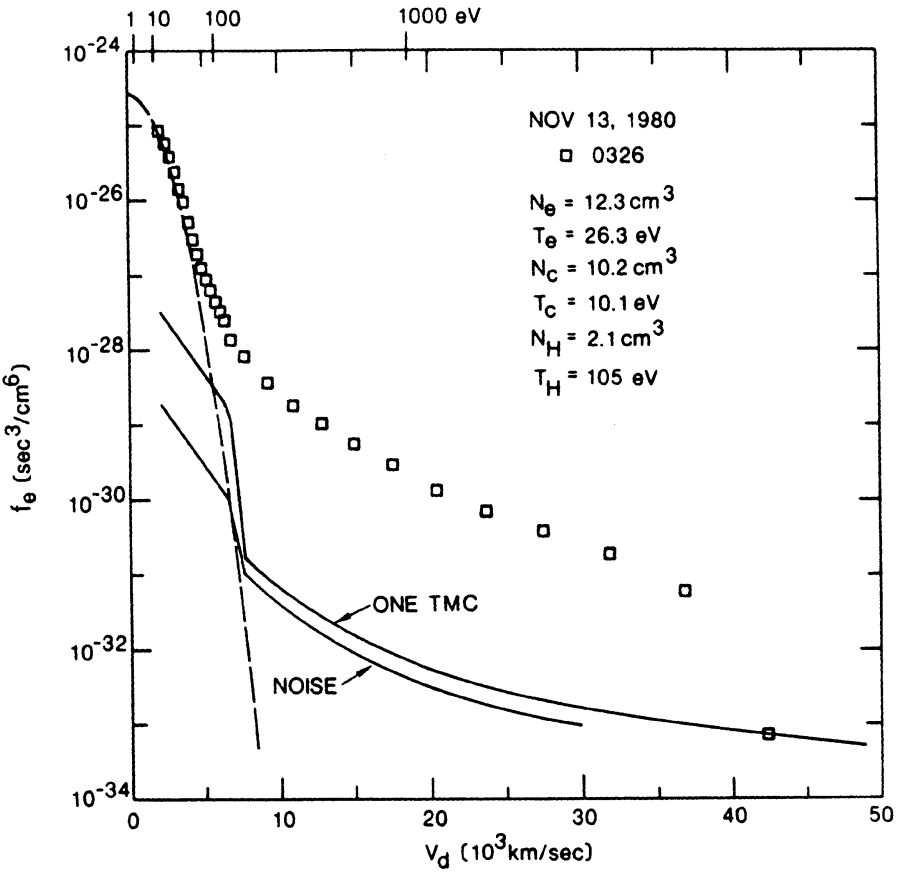

Fig. 5. Electron distribution function for 0326 UT, 13 November 1980, when Voyager 1 was outbound, approaching the ring plane near the Dione orbit. This shows the characteristic two-component spectrum, consisting of a suprathermal population and a cold distribution. Because the spacecraft was in ultraviolet ring occultation at this time, the spacecraft is negatively charged. Therefore, the computed electron density will be underestimated, which is probably down from the true value by a factor of 2 (see discussions in Sittler et al. 1983).

plasma temperature by nearly three orders of magnitude produces an observed increase in plasma sheet thickness of more than an order of magnitude with increasing radial distance from Saturn. Scale heights of cold heavy ions can be as low as 0.2 R_S in the inner magnetosphere and as high as 3 R_S in the outer magnetosphere. Many of the observed density variations can be attributed in part to changes in density scale height, with no need for a change in plasma flux-tube content.

In summary, Voyagers' plasma probe observations suggest that there are three fundamentally different plasma regimes: the hot outer magnetosphere, the extended plasma sheet, and the inner plasma torus. In the hot outer magnetosphere, densities range between $\lesssim 0.01$ cm^{-3} and 0.1 cm^{-3} and electron temperatures range between 50 eV and 800 eV. Near noon local time, the plasma electrons of the outer magnetosphere are reported to have a highly time-dependent behavior (Sittler et al. 1983), and the observed density enhancements are generally regions with enhanced levels of cold plasma. On the

average, 25% and 85% of the electron density and pressure, respectively, are partitioned to the suprathermals. Within the density enhancement where cold electrons are observed, cold high-Mach-number ions moving nearly in corotation directions are observed in the ion spectra. This highly time-dependent region, which resides outside the outer boundary of the extended plasma sheet, has been designated by Goertz (1983*a*) as a turbulence layer; the density enhancements have been attributed by Goertz to detached plasma "blobs" or "islands" which have broken off from the outer boundary of the plasma sheet because of the centrifugally driven flute instability. These density enhancements are subsequently (within a few rotation periods) lost down Saturn's magnetotail by way of a planetary wind mechanism, where Goertz has suggested that the low-density, hot-plasma regions measured by the low-energy charged particle (LECP) instrument (Maclennan et al. 1983) represent flux tubes recently emptied.

The extended plasma sheet is a region with enhanced levels of cold plasma relative to those detected in the hot outer magnetosphere. Densities range between 0.1 cm^{-3} and 2 cm^{-2} and electron temperatures range between 10 eV and 100 eV. Here, less than 15% of the density is partitioned to the suprathermals, although the suprathermals still contribute more than 80% of the electron pressure. Sittler et al. (1983) suggest that the extended plasma sheet is probably the primary contributor to the ring current modeled by the magnetometer team (Connerney et al. 1981), and estimate that a significant fraction of the ring current is probably produced by the low-energy plasma below 6 keV. Centrifugal stresses (dominated by cold heavy ions) and pressure gradients (dominated by hot ions) probably contribute equally to the ring current (see Lazarus and McNutt 1983).

The inner plasma torus is a region of reduced electron temperature $T_e < 10$ eV and scale height $H_i < 1$ R_S, with equatorial densities which can become as high as 100 cm^{-3}, and electron temperatures which can go as low as 1 eV. The inner plasma torus is also a region where the suprathermals are severely depleted relative to those in the extended plasma sheet; electron fluxes are generally confined below 50 eV compared to 6 keV in the extended plasma sheet. A strong attenuation of the suprathermals was observed inside $L \sim 5$ during the Voyager 2 encounter. Sittler et al. attributed this to the E Ring, which has an enhanced optical brightness or ring opacity inside $L \sim 5$ (Baum et al. 1980). Localized reductions in electron temperature and enhanced depletion of the suprathermal electrons were also observed near the L shell of Tethys, Dione, and possibly Rhea. These effects signify an interaction between the electrons and localized concentrations of dust, neutral gas, plasma ions and/or plasma waves centered on the satellite positions. The energy dependence of the depletions supports an interaction with dust or plasma waves in some cases, while in other cases an interaction with neutral gas or plasma ions is favored. The observed depletions of suprathermal electrons seem to be associated with the energy-dependent signatures of electron fluxes

$\sim$ 20 keV measured by the LECP instrument (Krimigis et al. 1981,1982*a*).

Recently, Lazarus and McNutt (1983) presented a detailed description of the Voyager measurements of plasma ions in Saturn's magnetosphere. The full analysis of these ion observations is extremely complex. The authors had to deal with questions of changing plasma composition, varying scale heights and velocities for different species, and non-Maxwellian (hot and cold) distributions for any given species. In addition, there were concerns about the degree to which the plasma ions were strictly corotating with the planetary magnetosphere, and in some regions model fits suggested that the radial flow was also significant.

It is not appropriate to provide a summary of these extremely complex discussions in this chapter; we refer the reader to the report by Lazarus and McNutt (1983) for further details. Here, we simply extract from the full report a brief discussion comparing the Voyager 1 and 2 ion measurements near the ring-plane/magnetic-equator crossing. The bottom panel in Fig. 6 is similar to a figure published in the Voyager 2 report by Bridge et al. (1982), showing a sequence of full ion spectra taken from 0000 to 1000 UT on 26 August 1981, as the spacecraft swept down from 2.2 R_S above the ring plane to 2.2 R_S below it. The relative currents detected by one sensor are plotted against energy-per-unit charge; it can be seen that near the beginning of this interval the ions were observed only in the first few E/Q channels. Bridge et al. (1982) suggested that these spectra are associated with cold protons, and they noted that the sudden decrease in the currents after 0130 UT is related to an abrupt change in plasma properties, such as a density decrease.

Centered about the ring-plane crossing there is a narrow but intense enhancement in currents for the lowest channels; Bridge et al. (1982) stated that these observations can be explained by assuming an O^+ plasma with ion density of $\sim$ 100 cm^{-3} and temperature near 10 eV. As indicated in Fig. 3, there were no measurable electrons at this time, suggesting $T_e < 1$ eV (Sittler et al. 1983; Lazarus and McNutt 1983).

The corresponding Voyager 1 plot is shown at the top of Fig. 6 (the side sensor is used because of a Voyager 1 roll manuever at 0044 UT; this is the interval with large currents in this figure). Simulations of some of these spectra with isotropic Maxwellian distributions convected with the rigid corotation velocity show that the Voyager 1 low-energy peaks in Fig. 6 are primarily H^+. Variations between the light and heavy ion peaks could be the result of noise or slight additions of very cold ions of high ionization states (e.g., O^{2+}, O^{3+}).

Lazarus and McNutt (1983) have shown that the proton number density reached its maximum at a distance of 1.15 R_S below the equatorial plane, with a thermal speed of $\sim$ 40 km s^{-1} ($\sim$ 8 eV) and a density of 15 cm^{-3} (this number may be an overestimate because of spacecraft charging). The heavy-ion peak was still increasing at this time. The inferred heavy-ion number density exhibited a broad maximum between 0300 UT (r = 5.0 R_S, z = -0.63

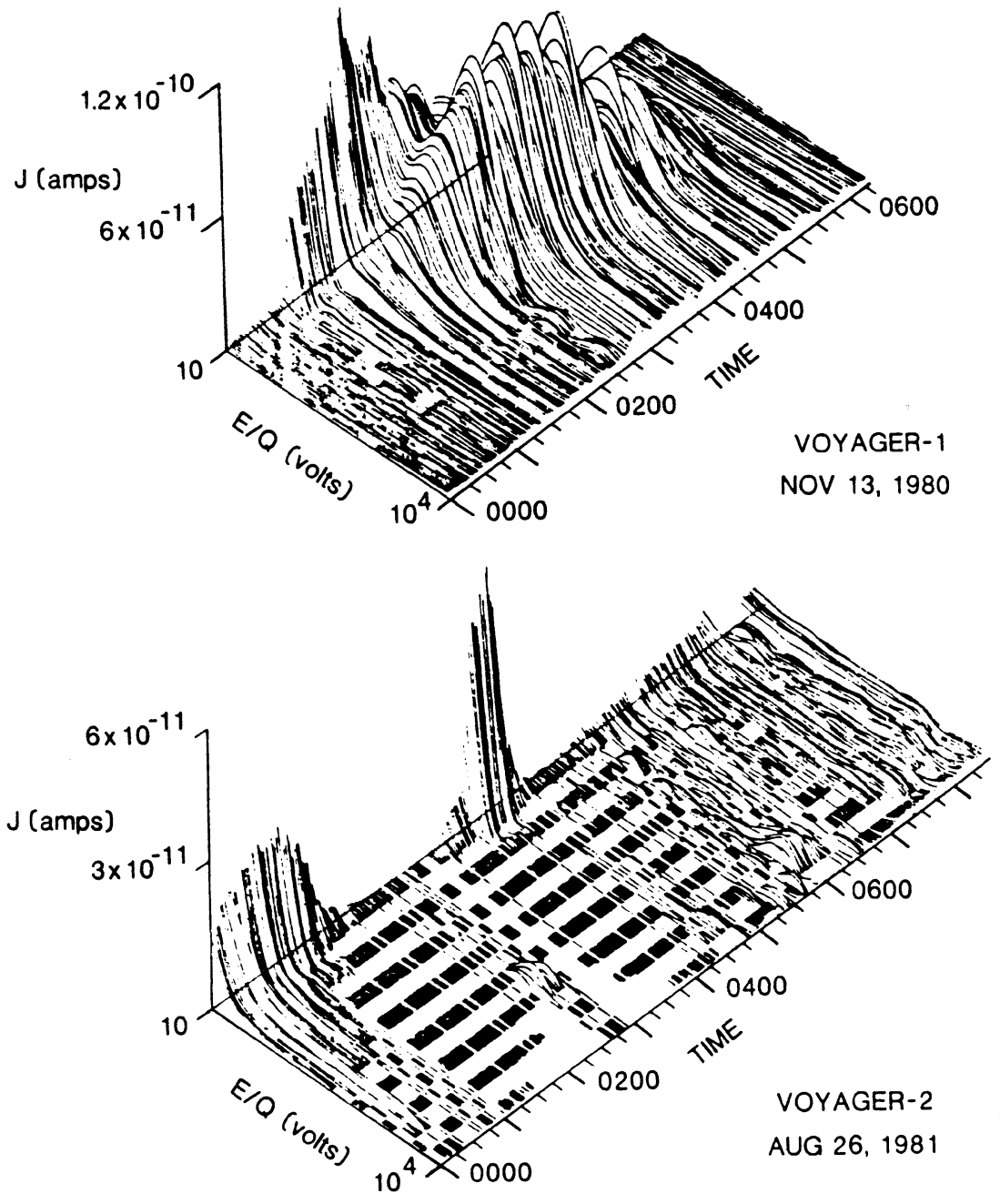

Fig. 6. Time-ordered sequences of ion spectra obtained as Voyager 1 (top) and Voyager 2 (bottom) crossed the ring plane/magnetic equator in the inner magnetosphere. In each scan, the relative current is plotted as a function of energy-per-unit charge.

R_S, $L = 5.1$) and 0400 UT ($r = 5.9\ R_S$, $z = -0.14\ R_S$, $L = 5.9$). This maximum occurs between Dione and Tethys and is consistent with these satellites being sources of plasma (Frank et al. 1980; Cheng et al. 1982; Lanzerotti et al. 1983*a*). The ion density is a function of radial distance from Saturn as well as of height above the ring plane. The ring plane was crossed at 0418 UT, just inside the orbit of Dione. There is no relative maximum in the density profile, which is consistent with the radial gradient in density being much greater than the gradient in z in this region.

The plasma ion results appear to be consistent with rigid corotation of the magnetosphere, and there is the possibility of more than one heavy ionic species. In a set of low-resolution spectra obtained at 0225 UT, Lazarus and McNutt found that a light-ion peak, a heavy-ion peak, and a possible warm-ion background were all visible.

The presence of a warm-ion component in the plasma science instrument (PLS) energy range is most prevalent in the outer magnetosphere (extended plasma sheet, hot outer magnetosphere). In the outer magnetosphere, for ion spectra that have been analyzed in detail, the warm-ion component dominates the ion pressure. The importance of the hot ions dominating the plasma pressure is reinforced by the significant ion pressures measured by the LECP instrument above 28 keV (Krimigis et al. 1983). As discussed in Lazarus and McNutt (1983) this warm component probably involves a heavy ion which is locally formed in the vicinity of the neutral hydrogen cloud. Sources of heavy neutrals in this neutral cloud are Titan and Saturn's main ring system (Eviatar et al. 1983). This hot-ion component probably makes a significant contribution to the ring current reported by Connerney et al. (1981), and the nearly coincident location of the ring current and the inner boundary of the neutral cloud at 8 R_S is probably not a coincidence (Sittler et al. 1983; Lazarus and McNutt 1983).

III. LOW-ENERGY RADIATION BELT PARTICLES

Pioneer 11 carried a number of instruments designed to study the characteristics of trapped radiation belts. Many details of these measurements are contained in the chapter by Van Allen in which he emphasizes particle interactions with the rings and the inner satellites. Figure 7 shows the buildup of electron flux and the characteristic hardening of the electron spectrum with decreasing distance from the planet. This also shows the electron cutoff at the ring boundary.

Krimigis et al. (1981,1982*a*) presented extensive preliminary discussions of the Voyager electron and ion measurements ranging down to low energies $\gtrsim$ 22 and 28 keV for electrons and ions, respectively. These Voyager measurements of low-energy particles greatly extend our knowledge of the physics of Saturn's magnetosphere. We refer the reader to initial reports for detailed discussions of the outer magnetosphere, the Titan encounter (see also Maclennan et al. 1982), and the traversals of the magnetopause and bow shock (Maclennan et al. 1983). In the remainder of this section we focus attention on the inner magnetosphere.

A comprehensive overview of the Voyager 1 electron and ion spectral intensities within approximately the orbit of Titan is presented in Color Plate 1. This plate shows differential ion and electron spectral intensities, respectively, as a function of time along the abscissa; the ordinates represent energy increasing downward, with the intensity color-coded in accordance

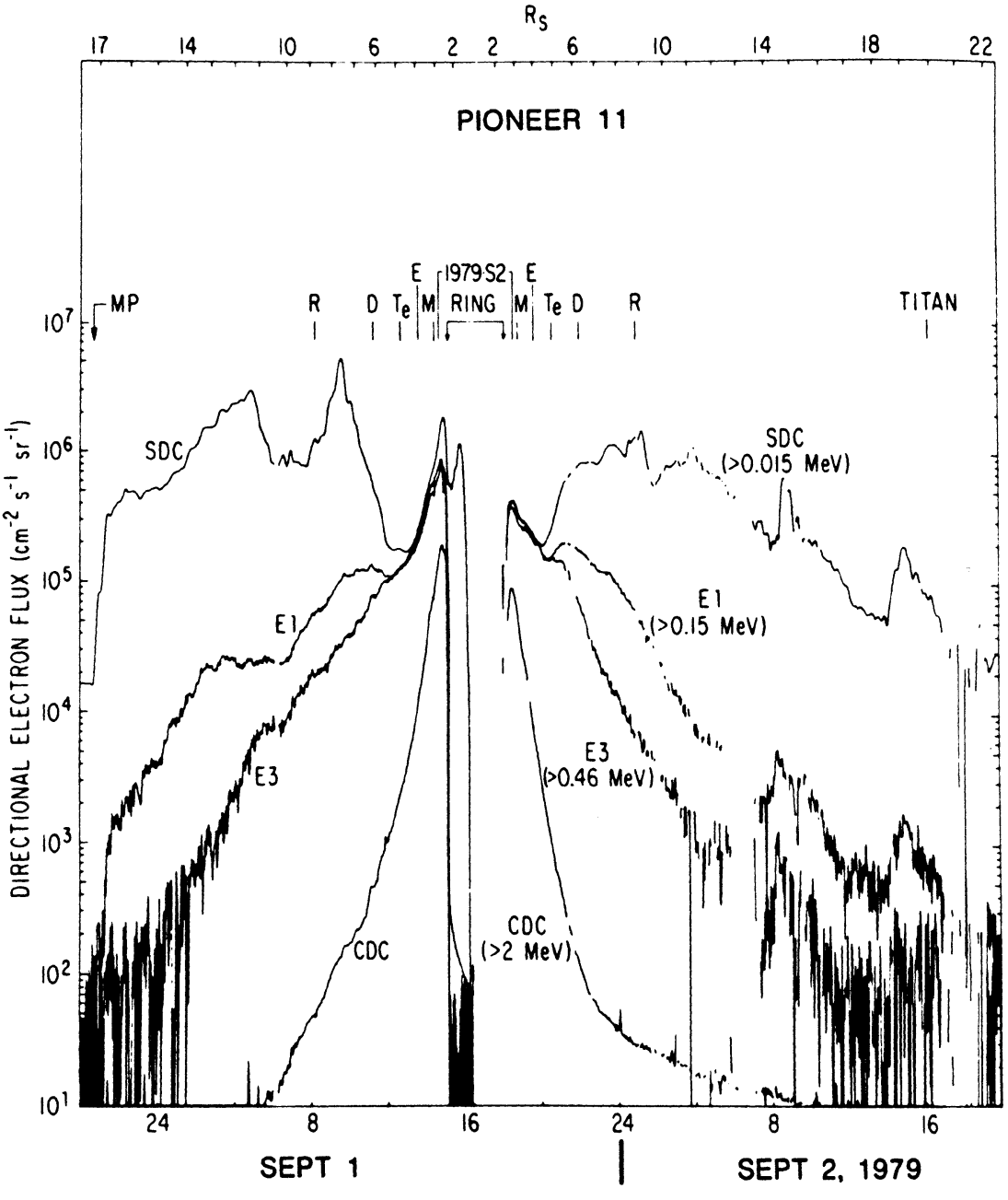

Fig. 7. Pioneer 11 measurements of equatorial profiles for locally mirroring particles. The magnetopause crossing is marked MP. As the spacecraft spins and the viewing orientation of the trapped radiation detector is perpendicular to the spin axis, the detectors become perpendicular to the magnetic field line twice during each spacecraft revolution, and the directional flux of particles with 90° pitch angle is shown here. Electron intensities above 4 thresholds are shown. The trace labeled SDC is a linear combinator of SPDC and SEDC outputs chosen to give the intensity of electrons only. As the detector is calibrated for energy flux (eV cm^{-2} s^{-1} sr^{-1}), an average energy of 15 keV was used to convert to number flux (cm^{-2} s^{-1} sr^{-1}). (See Fillius et al. [1980] for definitions of the channel names.)

with the color bars on the right-hand side. The ion data (15-min averages) have been smoothed using a logarithmic interpolation routine extending from ~ 40 keV to 1 MeV. The data have been corrected for background (Krimigis et al. 1983).

The decrease and recovery of the ion intensity at ~ 1015 UT (Day 317) have previously been interpreted as a feature of the boundary of the stably trapped region in the Saturn magnetosphere (Krimigis et al. 1981). Two other ion flux features particularly evident in the spectrogram are the sharp increase in intensity for energies ~ 150 keV beginning at the L shell of Rhea (peaking inside the orbit of Dione) and the relative depletion of 200 to 400 keV ions inside the orbit of Dione. The latter depletion was followed by a short recovery just before the crossing of the Tethys L shell (depletion of energetic ions $\gtrsim$ 80 keV). Between the orbits of Rhea and Tethys inbound the spectrum is relatively flat below ~ 100 keV, indicative of a hot plasma (Krimigis et al. 1983). The peak inside the orbit of Dione approximately coincides with the maximum in the low-energy electron density (Bridge et al. 1981*a*).

The electron spectrogram in Color Plate 1 (lower panel) has been constructed by applying a 5-point interpolation routine over the energy range 40 to 400 keV. The data have been corrected for background and averaged over 15-min intervals. The electron intensities varied considerably until Voyager entered into the durably trapped region at ~ 16 R_S at ~ 1015 UT on Day 317. The spectrum became progressively harder, especially inside the Rhea L shell. A sharp drop in low-energy electrons ($\lesssim$ 100 keV) occurred inside the orbit of Rhea. Depletion of fluxes was seen at the higher ($\gtrsim$ 150 keV) energies inside the Dione L shell and at the Tethys L shell. The electron intensities began to recover after Voyager crossed the Tethys L shell outbound, starting with the lower energies, progressing to higher energies, and reaching peak intensities at the orbit of Dione. In general the spectra become particularly hard at the higher (> 100 keV) energies between the orbits of Rhea and Dione, both inbound and outbound. For the Voyager 2 observations, we refer the reader to the chapter by Van Allen which gives a corresponding summary discussion.

In the initial Voyager 2 report (Krimigis et al. 1982*a*), it was noted that the low-energy (22–35 keV) electrons exhibited considerable variability between the orbits of Rhea and Dione during the inbound pass. A detailed plot of the electron and ion intensities around Rhea and Dione during this time is shown in Fig. 8 at the highest available time resolution of the instrument (0.4 s per plotted point). The bottom set of points in each panel, occurring every 6.4 min, represents a measure of the background counting rate. The foreground/background ratio for all three channels is usually > 10. The intensity fluctuations, largest at the lower energy, begin at the crossing of the Rhea L shell, continue through the Dione L shell, and terminate prior to crossing Tethys' L shell. The fluxes in the ion channel in the bottom panel do not show

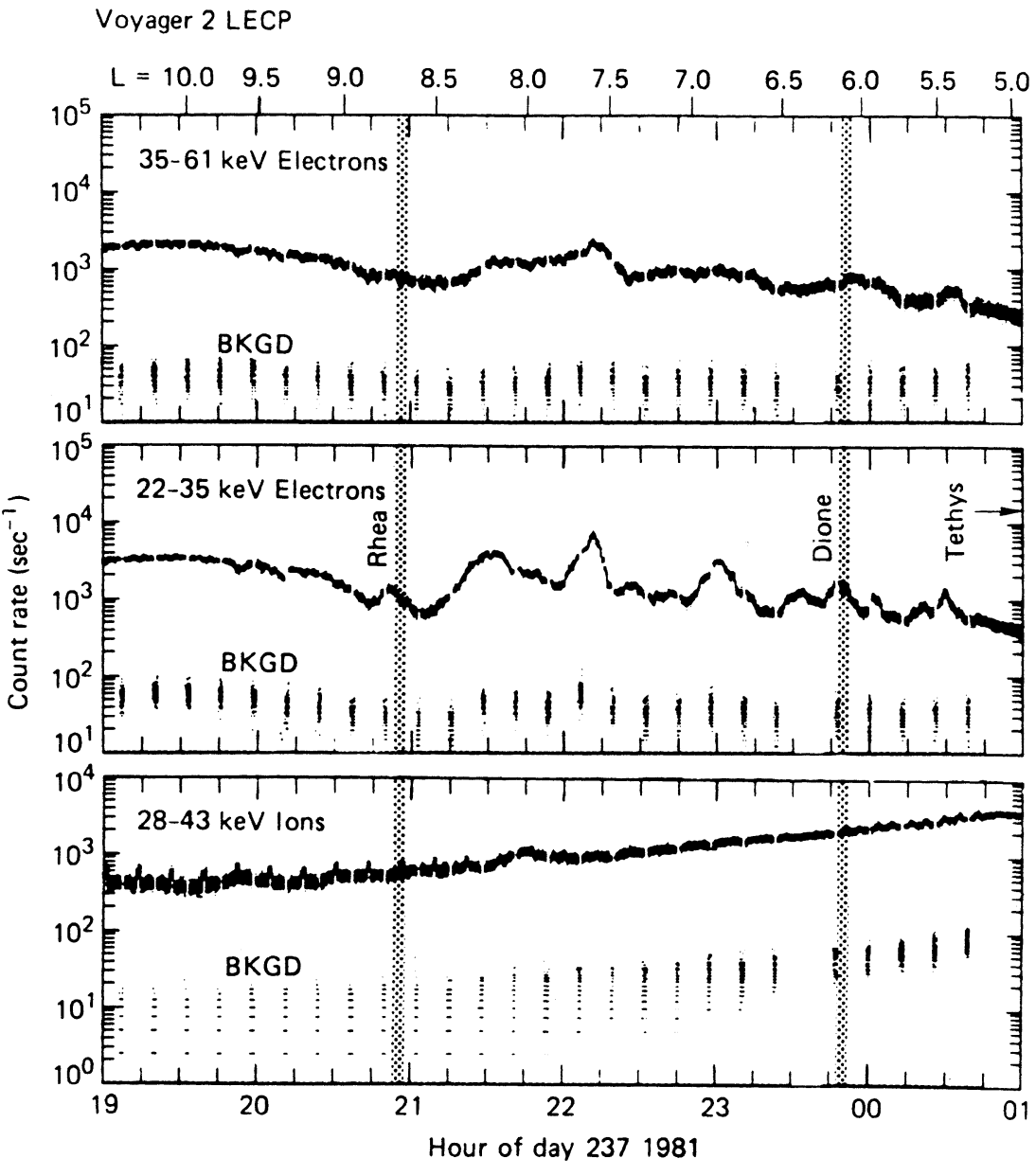

Fig. 8. An example of variable low-energy electron fluxes in the inner magnetosphere.

a variability similar to that of the electrons. Kurth et al. (1983) noted that these variations in electron rates are present in the general region where electrostatic waves are observed by the Voyager plasma-wave instrument (see Sec. IV).

A. Ion and Electron Spectra

The ion spectra observed by Voyagers 1 and 2 can be described well at lower energies by a Maxwellian distribution and at higher energies by a power law (Krimigis et al. 1981,1982*a*). A single expression used to fit the spectra is the *k* distribution (see e.g., Vasyliunas 1971)

$$f(\bar{v}) = \frac{n}{\pi^{3/2}\omega_0^2} \frac{\Gamma(k+1)}{k^{3/2}\Gamma(k-1/2)} \left| 1 + \frac{|\bar{v} - \bar{V}|^2}{k\omega_0^2} \right|^{-(k+1)} \quad (1)$$

where n is the particle density, $\bar{v}$ the particle velocity, $\bar{V}$ the bulk plasma velocity, and ω_0 (the most probable speed) is $\sqrt{2kT/M}$ where T is the plasma temperature and M is the particle mass. Using $j = p^2 f(\bar{v})$ where $j = dJ/dE$ is the differential ion intensity and p is the ion momentum for nonrelativistic particles

$$j(v, \phi) = \frac{nm^2v^2Q(k)}{\pi^{3/2}\left|\frac{2kT}{M}\right|^{3/2}} \left| 1 + \frac{v^2 - 2vV\cos\phi + V^2}{k(2kT/M)} \right|^{-(k+1)} \quad (2)$$

Here

$$Q(k) = \frac{\Gamma(k+1)}{k^{3/2}\Gamma(k-1/2)} \quad (3)$$

is approximately constant (0.90 to 0.97) for values of the exponent k ranging from ~4 to ~15. For $v \gg V$

$$j = j_0 \left| \frac{E}{kT} \right|^{-(k+1)} \quad (4)$$

a power law in energy. The Maxwellian distribution is a special case as $k \to \infty$.

Figure 9a shows hourly averaged ion spectra from Voyager 1 together with fits of Eq. (2) to the data points. The ions are assumed to be protons and are plotted at the appropriate proton energy. The values of L,B at the beginning and end of each hour interval are shown in the spectral plots.

The k function fits most of the observed distributions well. In the fits V was assumed to be equal to the corotation velocity ($V_c = 9.82\ R_S\ km\ s^{-1}$), although the fit is not very sensitive to the precise value. Typical values of n are in the range 10^{-2} to $10^{-3}\ cm^{-3}$ and, of course, include the contribution to the density from ions below the detector threshold.

Figure 9b plots ion spectra measured by Voyager 2. The spectra are substantially flatter at low energies than in the case of Voyager 1. The temperature values of kT are as high as 45 keV with corresponding values of k as high as 15, indicating that the spectrum can be characterized as mostly thermal at $L \sim 10$ (and at higher L as well; see Krimigis et al. 1983). The densities are in the same range as those observed by Voyager 1.

The functional forms of the electron energy spectra are different from those of the ions. Figure 10 shows a set of hourly-averaged electron spectra

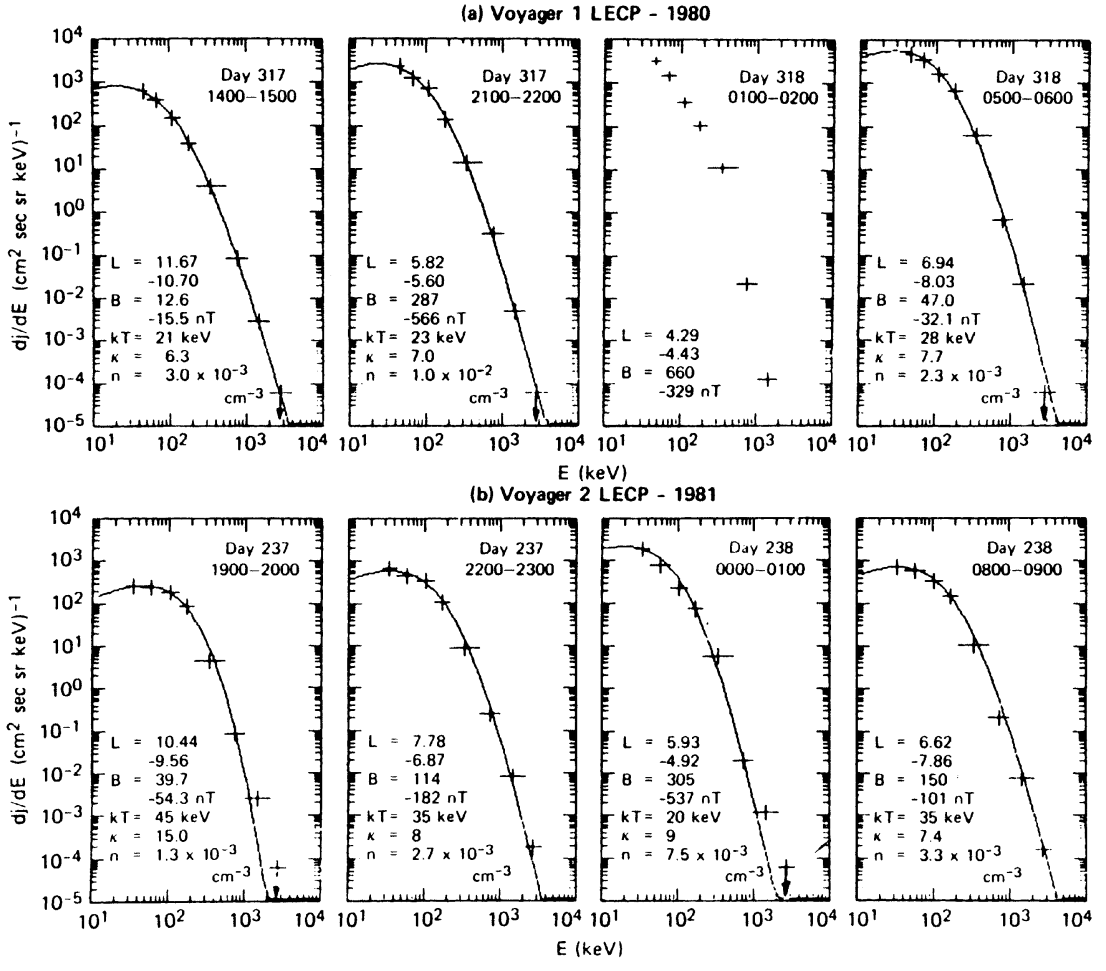

Fig. 9. Hourly averaged ion spectra from Voyagers 1 (a) and 2 (b), together with fits to the data points.

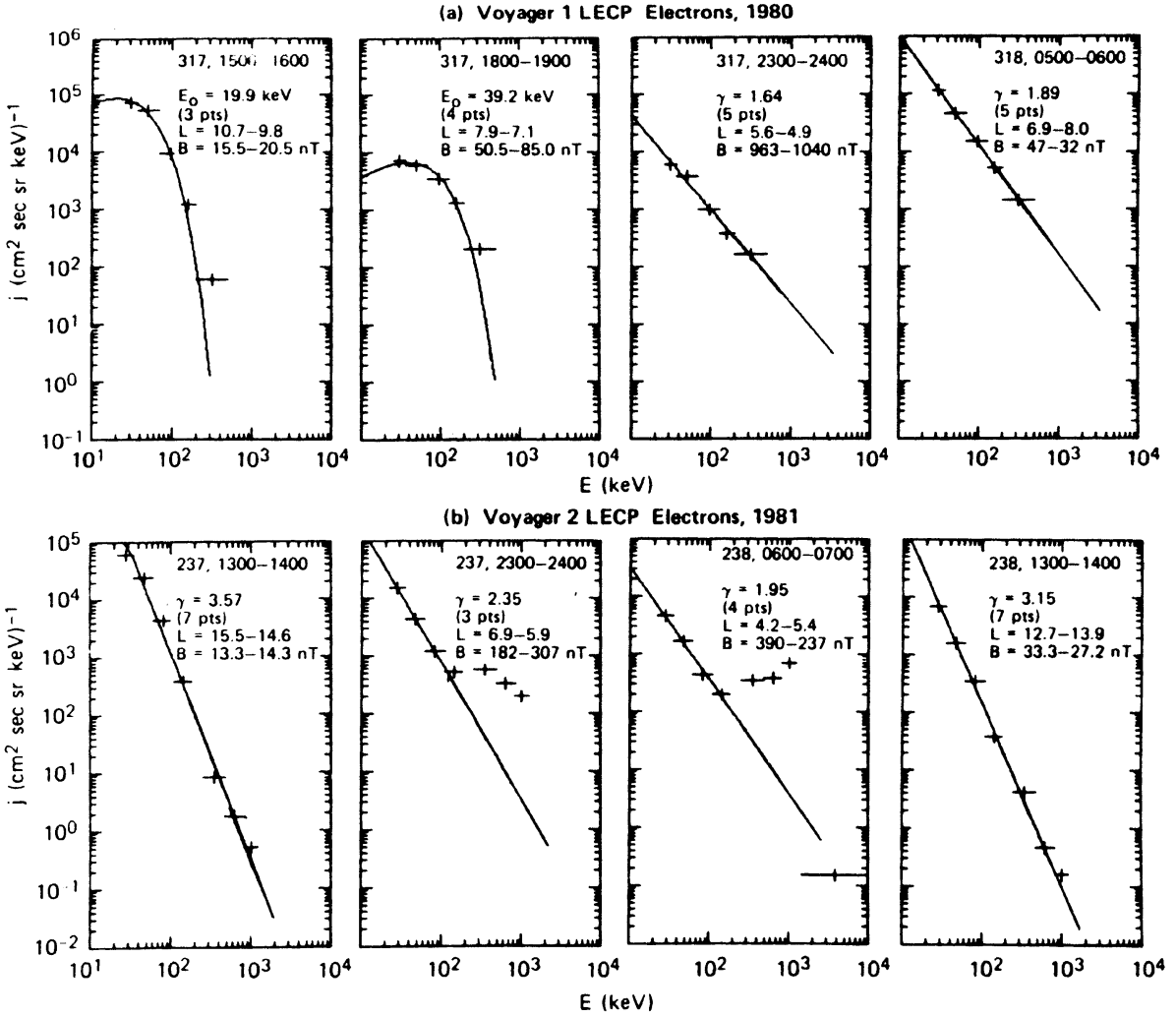

Fig. 10. Hourly averaged electron spectra from Voyagers 1 (a) and 2 (b).

for both spacecraft encounters at various L values. The data are fitted wherever possible to either a power law in energy

$$\frac{dJ}{dE} = CE^{-\gamma} \tag{5}$$

or an exponential of the form

$$\frac{dJ}{dE} = CE \exp(-E/E_0). \tag{6}$$

The Voyager 2 spectra (Fig. 10b) are best characterized by power laws, at least at the lower energies, whereas two of the Voyager 1 spectra are fit reasonably well by Eq. (5). In the Voyager 2 data (which had a broader electron energy coverage than did Voyager 1), at about the Dione L shell inbound, the spectra at low energies became substantially harder ($\gamma \sim 2.4$) and a secondary component began developing at energies $\gtrsim 200$ keV. This higher energy feature was present in the vicinity of the Tethys L shell outbound ($4.2 \leq L \leq 5.4$) as well, but exhibited a rather sharp drop above ~ 1 MeV. A similar spectral feature exists in the Pioneer data of McDonald et al. (1980).

The Voyager 1 and 2 trajectories in Saturn's inner magnetosphere crossed at four points in B,L space, inside the orbits of Dione and Tethys. Thus, the long-term (interval of ~ 9.5 months) variability of the fluxes of ions trapped deep within the magnetosphere of Saturn can be crudely assessed. Figure 11 shows a comparison of ion fluxes inbound at nearly identical points in B,L space. The Voyager 2 fluxes are lower almost everywhere than the intensities measured by Voyager 1, 286 days earlier. The decrease in intensity between the two encounters ranges from factors of 2 to 3 at the lower ($\lesssim 0.5$ MeV) energies to ~ 10 at the higher energies. Panels (a) and (b) include ions from a broad energy band (0.5–1.8 MeV) channel from the Pioneer encounter in September 1979 (Simpson et al. 1980*b*). Panel (c) contains Pioneer 11 measurements of McDonald et al. (1980). These Pioneer observations all show reasonable agreement with the Voyager results. Thus, there is a variability of ion fluxes over time deep within the magnetosphere, but an understanding of this will only come from detailed studies of the particle diffusion rates and sources. However, the existence of a variability does imply that the deep inner magnetosphere is not in a state of equilibrium.

B. Ion Energy Densities

The energy densities ε_i of the ions measured by the LECP instrument can be calculated as

$$\varepsilon_i = 4\pi \int_{E_t}^{E_{\max}} dE \frac{j_i(\bar{x},E)}{v_i} E_i \cong 4\pi \sum_{k=1}^{8} \left[\Delta E_i \frac{j_i(E)}{v_i} \bar{E}_i \right]_k . \tag{7}$$

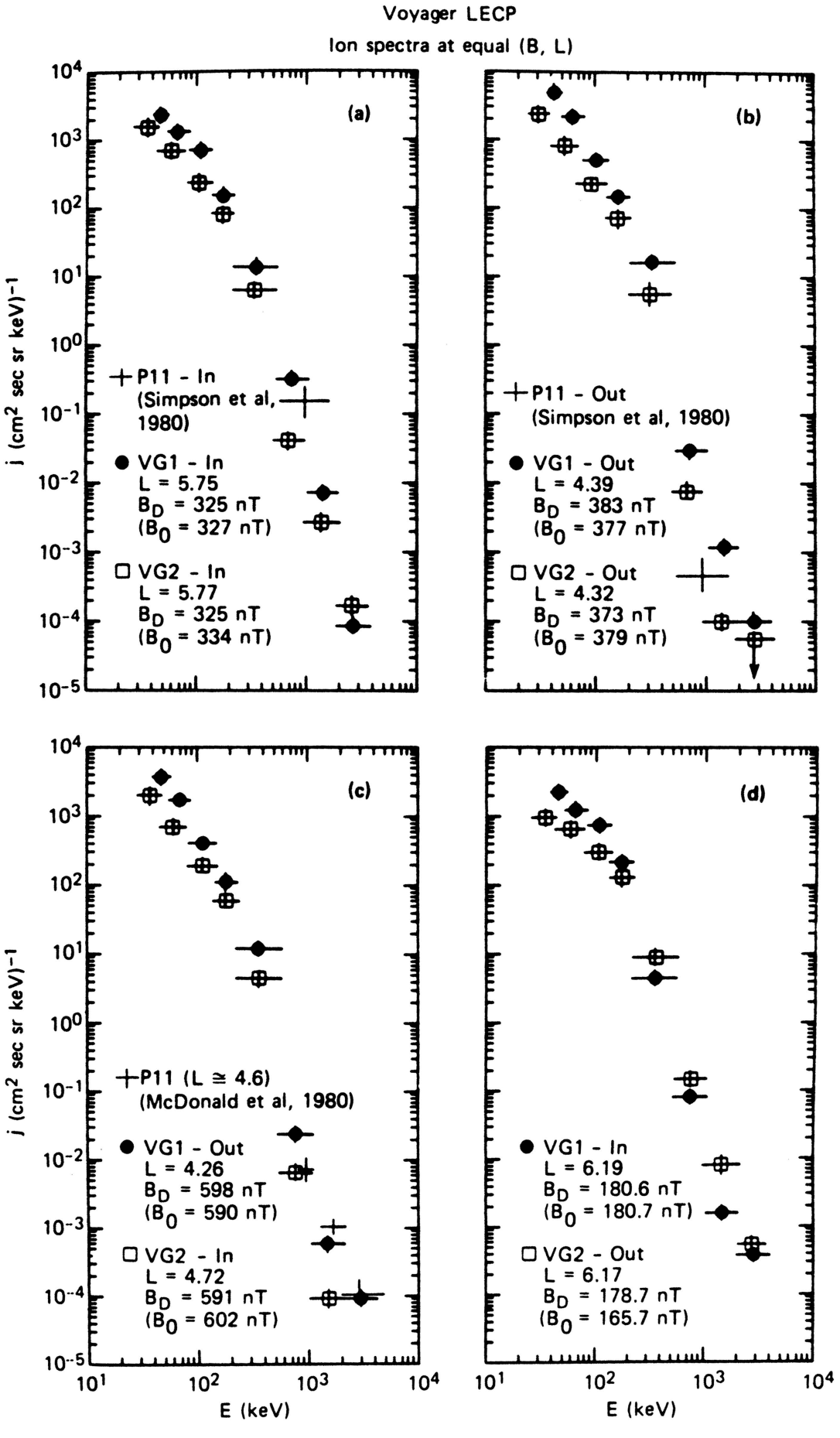

Fig. 11. Ion flux measurements from Pioneer 11, Voyager 1, and Voyager 2. The observations in each panel are associated with nearly identical values for B and L.

Discussions of this calculation as used for observations in the Jovian magnetosphere are given in Lanzerotti et al. (1980) and Krimigis et al. (1982*a*). Here, $\bar{E}_i$ is the mean energy of a particular ion channel, v_i is the ion velocity, j_i is the directional intensity, ΔE_i is the channel width, E_t and E_{max} represent the lower and upper energy thresholds of the detector, and $k = 1$ to 8 represents differential ion energy channels 1 through 8. Note that all quantities inside the brackets are known or are observables. Here, all ions are assumed to be protons, and scan-averaged intensities are used because the first-order anisotropy in Saturn's magnetosphere is quite small (Krimigis et al. 1981; Carbary et al. 1983*a*).

Figure 12 shows the proton energy densities for both encounters, together with the magnetic energy density $\varepsilon_M(B^2/8\pi)$ (Ness et al. 1981,1982*a*) and the resulting value of $\beta = (\varepsilon_p/\varepsilon_M)$. The details of the energy balance in the outer magnetosphere during both passes is given in Maclennan et al. (1983) and Lanzerotti et al. (1983*a*). In the outer magnetosphere the β value as determined from the ion measurements of the LECP instrument is quite large and, during Voyager 2, was observed to be $>> 1$ on one occasion (Maclennan et al. 1983). Inside $\sim 10\ R_S$ the proton β is small in both passes, inbound and outbound, except for Voyager 1 outbound, where β did not decrease until the orbit of Rhea. It is in this inner magnetosphere region that Frank et al. (1980) reported a high-β plasma detected by the plasma ion instrument on Pioneer 11. However, Krimigis et al. (1983) have noted that the LECP ion fluxes in this inner magnetosphere region are likely to consist of a large proportion of oxygen ions, in addition to hydrogen ions. For this situation, the total ion energy densities would be much larger than those estimated assuming only proton contributions. The total β of the inner magnetosphere would therefore have ion contributions from both the low-energy and high-energy plasmas and would likely be close to one in magnitude.

IV. PLASMA WAVE OBSERVATIONS

Although the Pioneer 11 payload did not contain a dedicated plasma wave investigation, measurements by the vector helium magnetometer showed that large-amplitude magnetic field oscillations, which could be interpreted as quasi-periodic electromagnetic waves, were present in a localized region near the Dione L shell. Figure 13 shows the three magnetic field components along with the field magnitude for one 12-min interval. Oscillations with a period of $\sim$ 15 to 20 s are evident in the figure. These transverse waves were identified as left-hand polarized ion cyclotron modes. Smith and Tsurutani (1983) pointed out that these waves could be expected to interact strongly with very low energy ions; for O^{++} and O^{+} the resonant ion energies would be $\simeq 300$ eV and $\simeq 5$ eV, respectively. Both Voyager spacecraft had electric field sensors and comprehensive plasma wave instruments covering the frequency

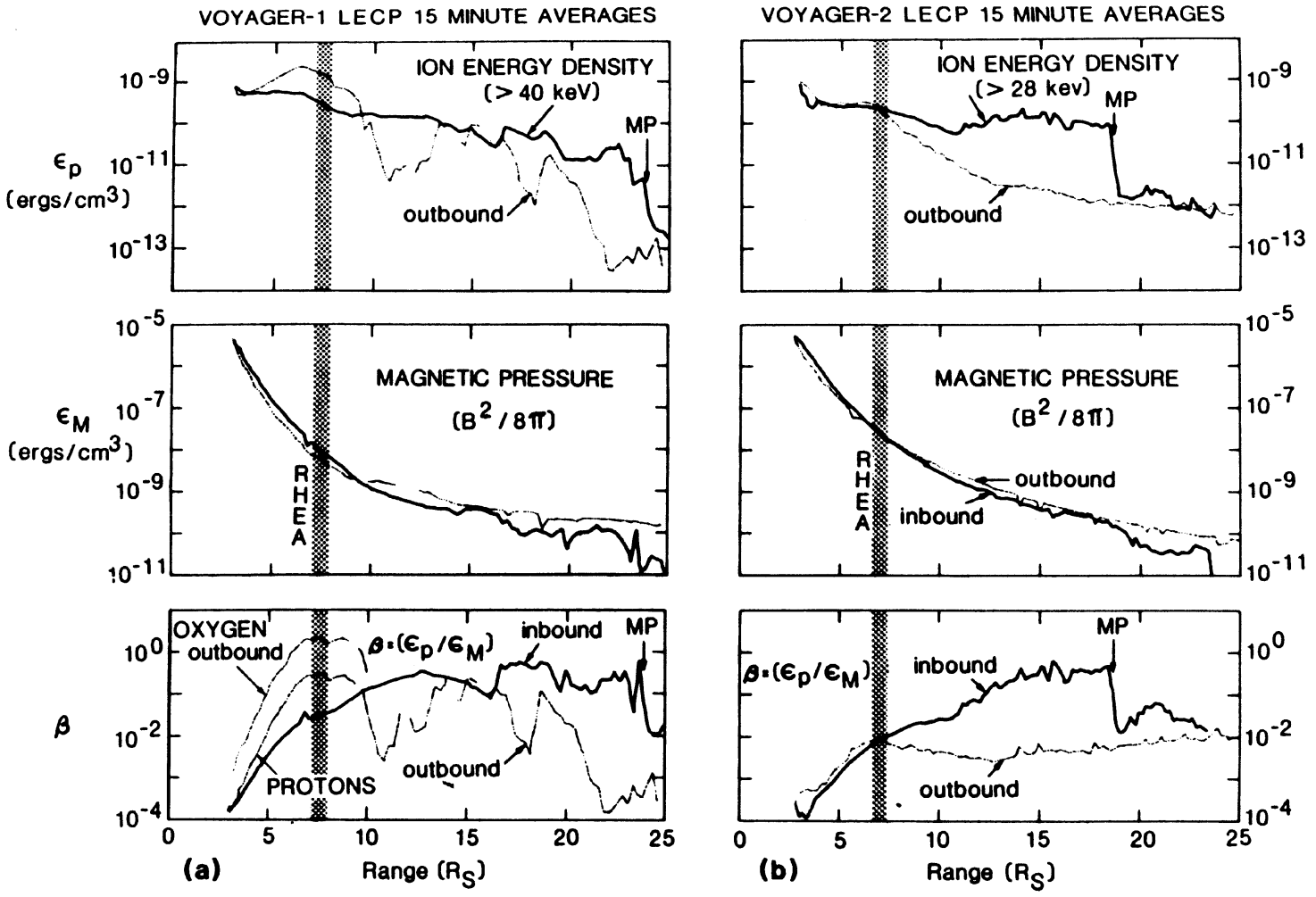

Fig. 12. Fifteen-minute averages of ion energy densities, magnetic pressure profiles, and energetic ion β variations for Voyagers 1 (left) and 2 (right).

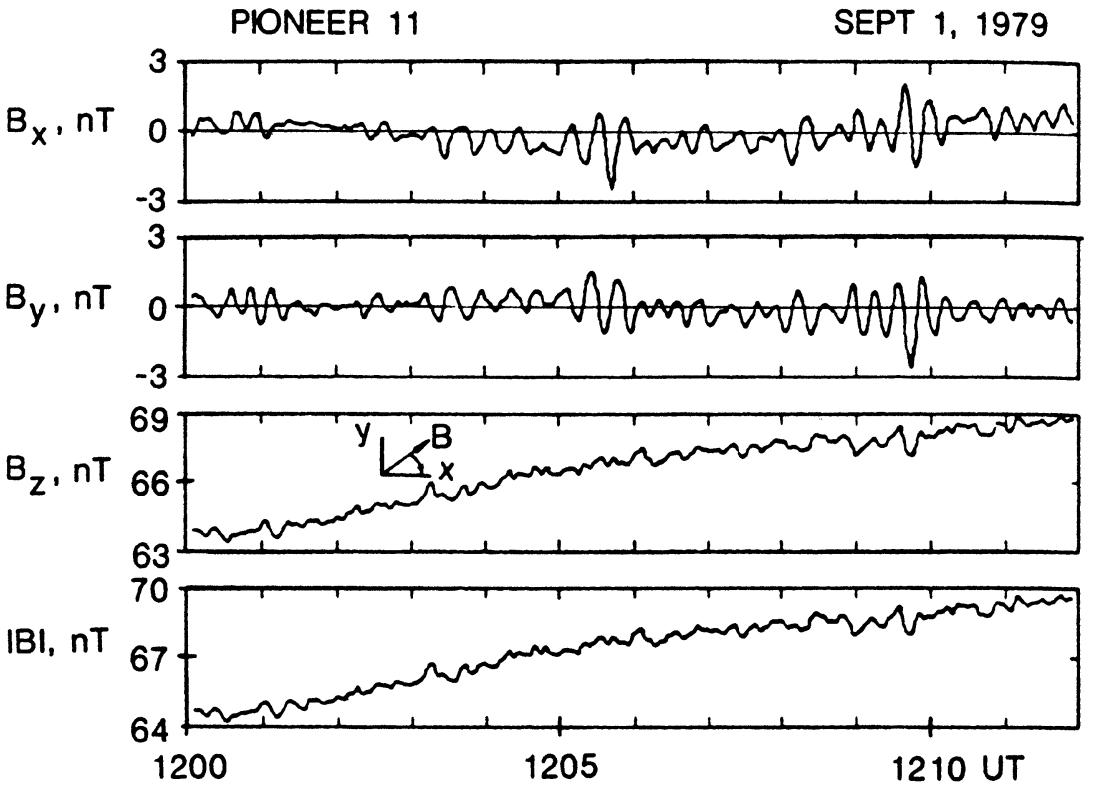

Fig. 13. Pioneer 11 observations of left-hand polarized ion cyclotron waves near the Dione L shell (figure from Smith and Tsurutani 1983).

range from 10 Hz to 56 kHz, plus radio astronomy instruments measuring wave activity up to a frequency of 40 MHz.

The initial reports on the Saturn plasma wave observations by Gurnett et al. (1981*a*) and Scarf et al. (1982) contained 24-hr plots of the Voyager 1 and 2 observations by the 16-channel spectrum analyzer centered about the times of closest approach. In each case, local values of the electron cyclotron frequency (f_c[Hz] = 28 B [gamma]) were derived from the magnetometer measurements (Ness et al. 1981,1982*a*), and f_c profiles were plotted along with the wave data. For Voyager 1, Gurnett et al. also provided a preliminary estimate of the electron plasma-frequency profile (f_p[kHz] = 9[N]$^{1/2}$, with N in cm^{-3}), derived largely from initial interpretations of the variations in wave intensity levels. A reanalysis of some high-frequency wave measurements by Pederson et al. (1981) suggested modifications in this density profile, and subsequent detailed studies by members of the Voyager plasma science team (Sittler et al. 1983) yielded greatly improved local electron density estimates. However, as noted by Sittler, the available results of the plasma probe still contain uncertainties caused by the presence of very cold electrons (which are not measured directly by the instrument), as well as by effects associated with spacecraft charging, deviations in ion flow direction, and variations in ion composition, all of which introduce problems in data analysis not easily re-

solved. Nevertheless, the electron measurements yield straightforward lower bounds for N, and these lower bounds, provided by the Voyager plasma team (see Fig. 3), were used to construct new f_p profiles shown in Figs. 14 and 15 for both encounters; Fig. 16 contains an unlabeled composite of the two wave data sets that provides a direct basis for comparison of the different inner magnetosphere traversals.

For the first 10-hr period on 13 November, the Voyager 1 f_p profile in Fig. 14 differs considerably from the preliminary one shown by Gurnett et al. (1981*a*). Since plasma wave modes are identified by comparing the wave frequencies with local values for f_p and f_c, it is appropriate to review the Voyager 1 analysis using the new density curve. We note that at low frequencies ($f \leq 1.0$ kHz) the intense wave activity in Fig. 14 has $f < f_c$, $f \ll f_p$ and is peaked near the magnetic equator (ring-plane crossing) with a secondary maximum near closest approach. Gurnett et al. (1981*a*) designated these emissions as "hiss and chorus," and Sittler et al. (1983) noted an association between these waves and fluxes of suprathermal electrons with energies be-

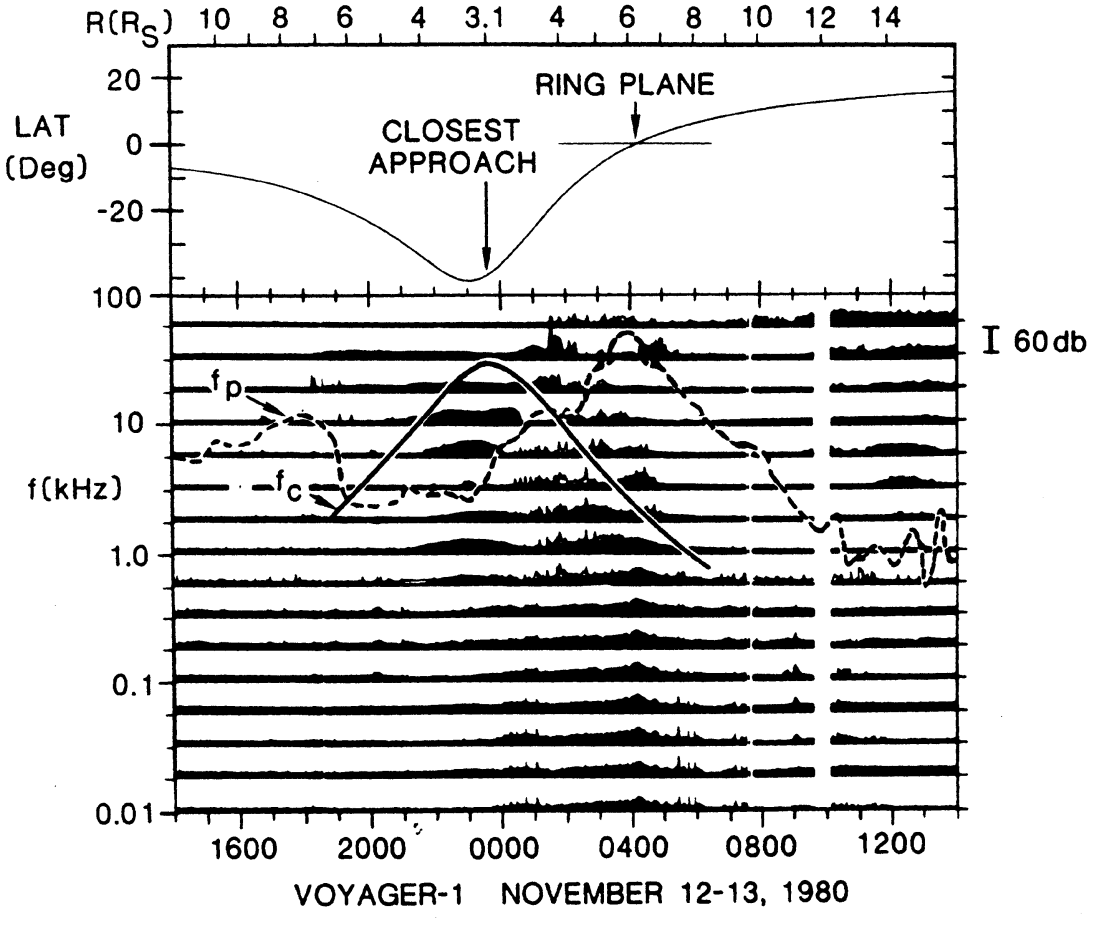

Fig. 14. Voyager 1 observations of the 16-channel spectrum analyzer for the 24-hr interval centered about closest approach. The f_c curve is derived from magnetometer data, and the f_p curve, derived from the plasma electron measurements, may represent a lower bound.

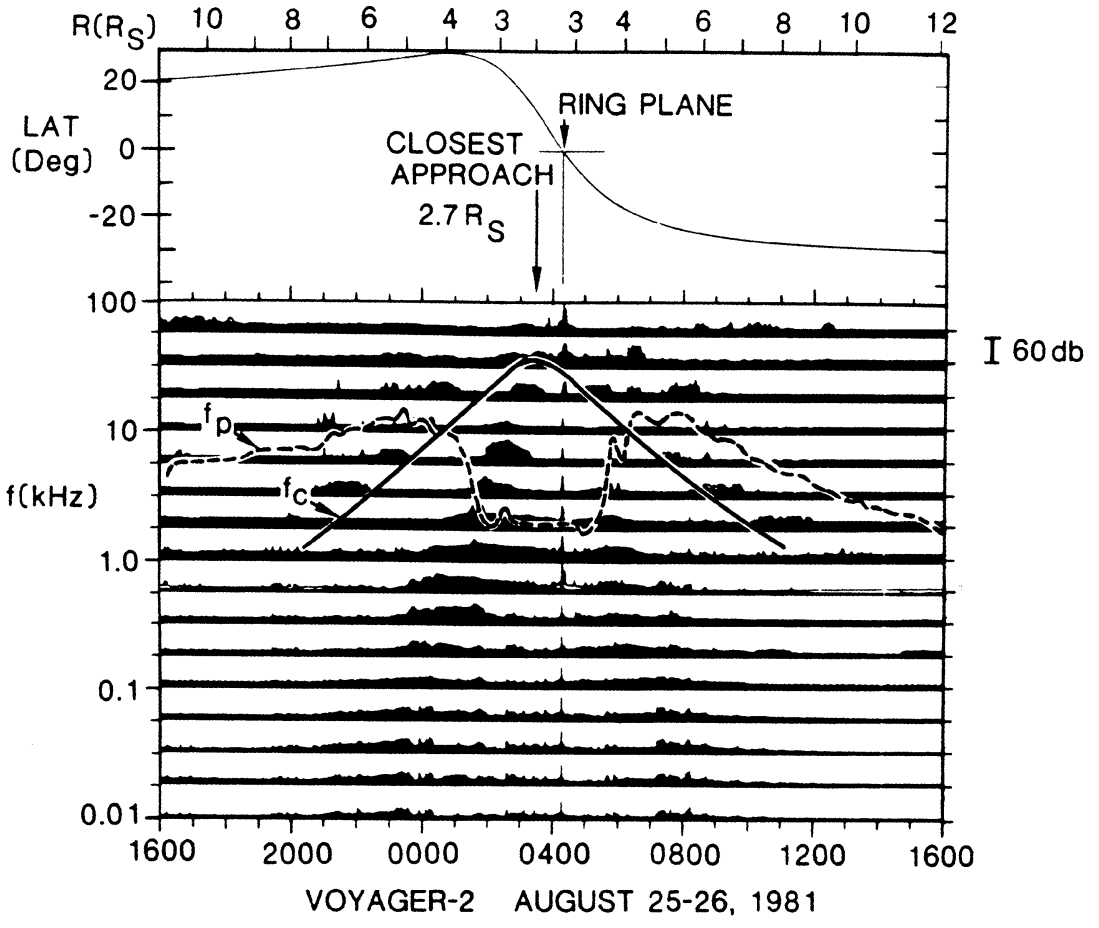

Fig. 15. Same format as in Fig. 14 for Voyager 2.

low 6 keV; this whistler mode identification is not affected by the changes in f_p. Similarly, the $(n + 1/2)f_c$ band designation for the 3 kHz enhancement near 0430 UT and the 5.6 kHz burst at 0300 UT, as well as the radio emission designation for the high-frequency waves (3.1 kHz $\leq f \leq$ 56 kHz) detected after 1000 UT, are unaffected by the change in the density curve. However, the new f_p profile is not in accord with some of the other identifications noted in the preliminary discussion by Gurnett et al. (1981*a*), particularly for the intervals near 0100–0200 UT (13 November) and 1800–2230 UT (12 November).

The initial plasma wave report of Voyager 1 contained the following analysis for the 12 November encounter interval: (a) brief noise bursts were detected in the 10 kHz and 17.8 kHz channels between 1800 and 2000 UT inbound, and these impulsive events had characteristics of electron plasma oscillations; (b) after 2000 UT, a band of intense steady emissions was identified with a well-defined lower cutoff that first decreased smoothly from 10 kHz (at 2030 UT) down to 3 kHz (at 2300 UT), and then increased in frequency. It was conjectured that these waves were electromagnetic; it was

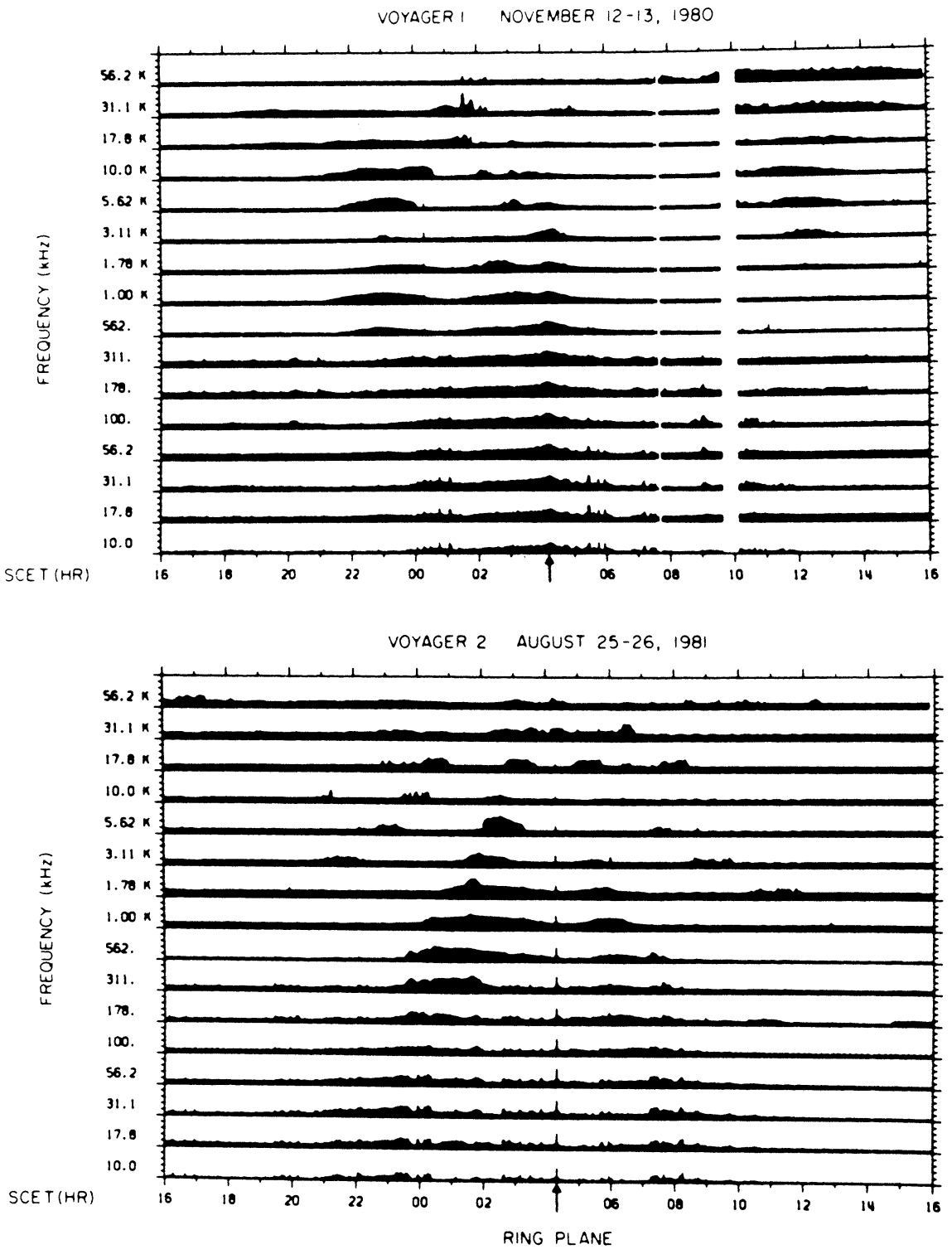

Fig. 16. Comparison of 16-channel measurements of Voyagers 1 (top) and 2 (bottom) in the vicinity of the ring plane/magnetic equator.

natural to assume that the smoothly varying lower cutoff represented a propagation cutoff at the local value for f_p.

A Voyager 1 wideband frame was recorded at 2252 UT on 12 November, showing that this radio emission had a very unusual spectral structure which contained a sequence of many narrowband emissions rather than the expected continuum. Gurnett et al. (1981*b*) used data from several additional wideband frames to show that the narrowband electromagnetic emissions were detected sporadically by Voyager 1 out to 59 R_S during the outbound leg. It was suggested that the waves were generated by conversion of intense electrostatic waves to electromagnetic emissions in inner magnetospheric regions with strong plasma density gradients, although no definitive evidence for such a steep gradient was available. More recently, Gurnett et al. (1982*a*) analyzed Voyager 1 wideband data showing similar narrowband emissions at Jupiter. A generation process to produce such emissions appears to be a common one in both planetary magnetospheres.

The f_p profile shown in Fig. 14 does not explain the impulsive noise bursts measured between 1800 to 2000 UT on 12 November, or the low-frequency cutoff of the narrowband emissions observed between 2000 and 2300 UT. Moreover, on the basis of experience in the Earth's magnetosphere, Gurnett et al. (1981*a*) identified the very intense 31 kHz noise burst at 0130 UT (13 November) as an upper hybrid resonance emission. However, this identification is also quite inconsistent with the f_p profile in Fig. 14. It might be considered that (unmeasured) cold electrons were present in sufficient numbers to yield significantly higher total densities. However, between 1900 and 2300 UT it appears that the electrons were warm enough to be measured; the plasma probe data yield $T_c \lesssim 3$ eV, $n_e \approx 0.5$ cm^{-3}, and $f_p \approx 6.3$ kHz. Thus, it can be concluded that the intense 31 kHz noise burst near 0130 is *not* an upper hybrid resonance emission. We have elaborated on this point to illustrate the present lack of understanding of several prominent wave emissions detected at Saturn.

It is known that very cold electrons must have been present during a part of the Voyager 2 encounter. As noted above (see Fig. 6), a high ion density was detected at the ring-plane crossing (Bridge et al. 1982), but the measured electron density was low. Thus, the f_p curve in Fig. 15 gives only a lower bound near the equator. However, for Voyager 2 there appear to be no serious problems associated with the new f_p profile beyond $L = 5$. For instance, Scarf et al. (1982) used upper hybrid resonance identifications to derive $f_p \approx 5.6$ kHz at 1640–1700 UT, $f_p \approx 10$ kHz at 2040–2120 UT, and $f_p \approx 18$ kHz at 2235–2315 UT. These values agree reasonably well with minimum values derived from the Voyager 2 plasma probe (note that the electron temperature was relatively high here). Moreover, the Voyager 2 detection of intense narrowband emissions at 5.6 kHz started just after 0202 UT, and this onset occurred fairly soon after a sharp dip in f_p. At 0200 UT, Lazarus et al. (1983) reported an H^+ density near 0.4 cm^{-3}, which gives $f_p \sim 5.6$ kHz; the density

profile probably fell well below 0.4 cm^{-3} until the ring-plane crossing. Thus, one might relate the emission onset to the spacecraft motion into a propagation region where the local cutoff frequency was below the wave frequency. Figure 15 also shows Saturn kilometric radiation, $(n + 1/2)f_c$ bands, and whistler mode chorus and hiss. Detailed discussions of the electrostatic wave observations are contained in a report by Kurth et al. (1983).

Before proceeding with a discussion of wave-particle interactions, it is necessary to comment briefly on Voyagers' impulsive wave measurements near the ring-plane/magnetic-equator crossings. At Jupiter, it was possible to identify certain impulsive signals as Doppler-shifted ion acoustic waves that appeared to interact strongly with low-energy ions (Scarf et al. 1981*b*). We considered similar explanations for the Saturn ring-plane observations. However, Scarf et al. (1982) used high-resolution wideband measurements (one point per 35 microsec; see bottom panel in Color Plate 2) to show that noise impulses of this type represent dust impacts rather than plasma waves. In a related work, Gurnett et al. (1983) used the detailed observations by the plasma wave instrument to deduce significant characteristics of the ring particles impacting the spacecraft. Scarf et al. (1983) noted that similar impacts were detected on Voyager 1 near the ring plane and at other locations.

V. CHORUS AND ELECTRON SCATTERING

Figure 17 illustrates in detail how the 16-channel wave levels varied during the Voyager 1 ring-plane/magnetic-equator crossing. Here, the calibrated and unaveraged field amplitudes are plotted, and the new f_p curve (based on the Pedersen et al. [1981] analysis and electron plasma probe measurements [Sittler et al. 1983]), is again superimposed. The f_c, $3f_c/2$, and $5f_c/2$ curves generally serve to order the higher frequency noise bursts in terms of $(n + 1/2)f_c$ bands (f_c being the electron cyclotron frequency), but between 0100 and 0230 UT the variations in the 17.8, 31, and 56 kHz channels cannot be completely explained in terms of ordinary electron gyroharmonics.

At 0326 UT a wideband frame was recorded, and the color-coded spectrogram (Color Plate 3) shows that for this interval weak electron gyroharmonic bands and strong hiss and chorus were present. The 48-second-long spectrogram is actually made up of 800 successive spectral scans; the left side of Color Plate 3 contains a 0.6-second average of ten of these scans. This plot shows clearly that three fairly weak $(n + 1/2)f_c$ emissions were detected along with strong banded chorus and somewhat weaker hiss. The term chorus is used because the waves are banded with $f \lesssim f_c/2$ and have characteristic rising frequency versus time structures. Although the temporal variations may appear unusually slow, Burtis and Helliwell (1976) have described observations of similar emissions in the Earth's magnetosphere. The detailed structure of the Saturn chorus is displayed in the upper panel of Color Plate 2. Color Plates 2 and 3 show that the chorus bandwidth is several hundred Hertz and

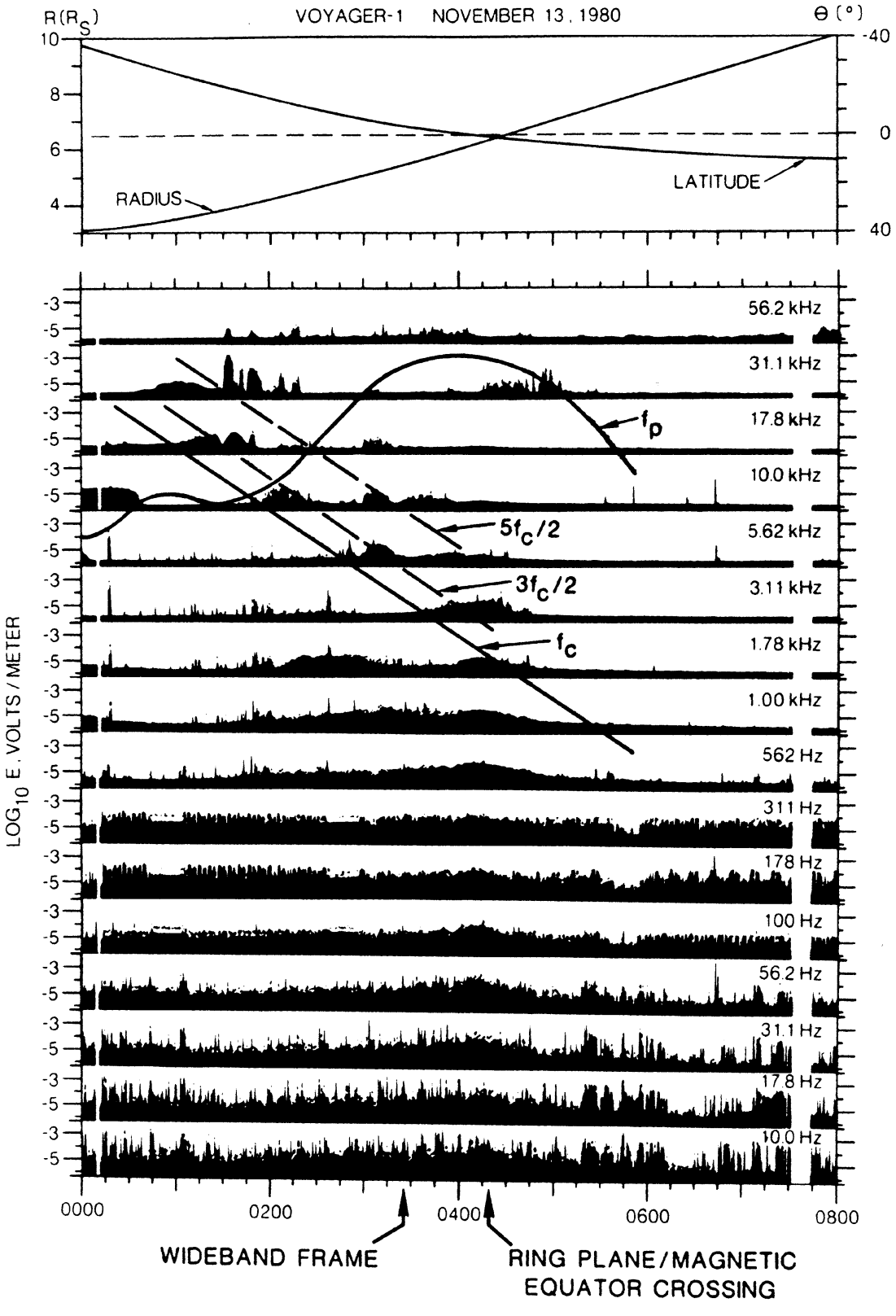

Fig. 17. Detailed plot of the Voyager 1 spectrum analyzer measurements near the outbound crossing of the ring plane and magnetic equator.

that the amplitude is orders of magnitude greater than for any of the $(n + 1/2)f_c$ modes.

Within the Io torus at Jupiter, Scarf et al. (1979), and Thorne and Tsurutani (1979) demonstrated that the whistler mode turbulence could be expected to produce significant loss of radiation-belt electrons. Subsequently, Coroniti et al. (1980) identified Jovian chorus in the Voyager data and showed that ~ 6 ergs cm^{-2} s^{-1} of electrons with energies on the order of a few keV would be precipitated into the atmosphere by whistler mode waves. For a quantitative analysis of the expected effects of Saturn chorus emissions, we consider the 1 kHz measurements at 0326 UT. Whistler mode waves that propagate parallel to the B field have an index of refraction n given by

$$n^2 = 1 + \frac{f_p^2}{f(f_c - f)} . \tag{8}$$

At 0326 UT, B was 120 γ while N was near 20 cm^{-3} (Sittler et al. 1983); thus $f_c = 3.36$ kHz, and $f_p = 40.25$ kHz so that $n(1\text{ kHz}) \approx 26$. The measured average E-field amplitude at 1 kHz was 1.76×10^{-6} V/m$(\text{Hz})^{1/2}$; thus B' (the magnetic field amplitude of the wave) was nominally equal to 1.54×10^{-4} $\gamma/(\text{Hz})^{1/2}$.

The whistler mode waves resonate with the cyclotron motions of electrons having (see Coroniti et al. 1980)

$$\frac{\text{v(res)}}{c} \cong \frac{f_c - f}{nf} \tag{9}$$

and the resultant pitch-angle diffusion coefficient $D_{\alpha\alpha}$ is

$$D_{\alpha\alpha} \cong \frac{1}{4}\left[\frac{e}{mc}\ 10^{-5}B'(f)\right]^2 \cdot \frac{f}{f_c + 2f} . \tag{10}$$

For $f = 1$ kHz, these expressions yield v(res) $= 2.55 \times 10^9$ cm s^{-1}, E(res) $= 1.85$ keV, and $D_{\alpha\alpha} = 3.5 \times 10^{-5}$ s^{-1}.

If we assume, as in the analysis for Jupiter, that the wave-particle interaction region extends over two Saturn radii along a flux tube centered at the magnetic equator, the bounce-average precipitation lifetime can be estimated to be $T_L \approx (\pi L/2)/D_{\alpha\alpha} \approx 2.5 \times 10^5$ s. The minimum precipitation lifetime is $T_M = 2L^4 R_S/v$ (Coroniti et al. 1980), which gives $T_M \approx 4000$ s; thus $T_M/T_L \approx 0.016$.

This very small value for T_M/T_L near the Saturn ring-plane crossing indicates that such wave-particle interactions would produce only weak diffusion and negligible precipitation. In order to assess this result, it is useful to recall that Coroniti et al. (1980) found $T_M/T_L \approx 0.3$ for Jovian chorus, while Scarf et al. (1979), and Thorne and Tsurutani (1979) found $T_M/T_L \approx 0.01$ to 0.2 for

Jovian whistler mode hiss. The weak diffusion result for Saturn appears to be quite consistent with electron measurements from the Voyager 1 plasma probe. Figure 5 yields $J(2.0\ \text{keV}) \approx 5 \times 10^5$ electrons $\text{cm}^{-2}\ \text{s}^{-1}$ at 0326 UT, while the stable trapping limit is near $10^7\ \text{cm}^{-2}\ \text{s}^{-1}$. Thus, we should not expect strong diffusion or large precipitation fluxes.

VI. ELECTROSTATIC WAVES AND WAVE-PARTICLE INTERACTIONS

In the preceding sections, the existence of upper hybrid resonance emissions, electron plasma oscillations (Langmuir waves), and electron cyclotron harmonic waves in Saturn's inner magnetosphere was noted. Recently, Kurth et al. (1983) conducted a comprehensive study of these electrostatic waves at Saturn, and summarized all of the Voyager observations. It is of interest to evaluate the wave-particle interactions that could be associated with the electron cyclotron harmonic waves in particular, since at Earth these waves are thought to contribute to the diffusion of electrons into the loss cone to produce the diffuse aurora (Kennel et al. 1970; Lyons 1974).

Current theories for the generation of the electron cyclotron harmonic waves require electron distribution functions with two (or more) components; the analysis is based on the Harris dispersion relation (Harris 1959) for electrostatic waves propagating in a hot plasma with an imbedded magnetic field (Ashour-Abdalla and Kennel 1978; Hubbard and Birmingham 1978; Rönmark 1978). Young et al. (1973) demonstrated that relatively weak loss-cone distributions are unstable to the electron cyclotron waves, provided a cold electron component accompanied the hotter component possessing a free-energy source. The free-energy source apparently can take a variety of forms (Kurth et al. 1979; Kurth et al. 1980) but must have a positive slope with respect to $v_\perp$, i.e. $\partial f/\partial v_\perp > 0$.

At Earth, the free-energy source is thought to involve electrons in the range from about one to several keV (Rönmark 1978; Kurth et al. 1979; Kurth et al. 1980*b*); hence, the existence of $(n + 1/2)f_g$ emissions at Saturn could, in principle, imply substantial fluxes of 1 to 10 keV electrons with $\partial f/\partial v_\perp > 0$. Indeed, above 22 keV there is evidence for large electron fluxes in Saturn's inner magnetosphere. Figure 18 shows a portion of the LECP data discussed in Sec. III.A (Fig. 9), with plasma wave data added.

The variations observed in the count rate from the unshielded sectors probably represent temporal changes (Krimigis et al. 1982*a*,1983). Krimigis et al. (1982*a*) analyzed the electron data shown in Fig. 18 by comparing the rates in two mutually perpendicular directions and found similar intensities, suggesting a nearly isotropic pitch-angle distribution. They further argued that the temporal variations at electron energies $\lesssim 60$ keV may be evidence of electron acceleration. Kurth et al. (1983) speculated that a weak loss-cone feature could be present in the energetic electrons and argued that the 22 to 35

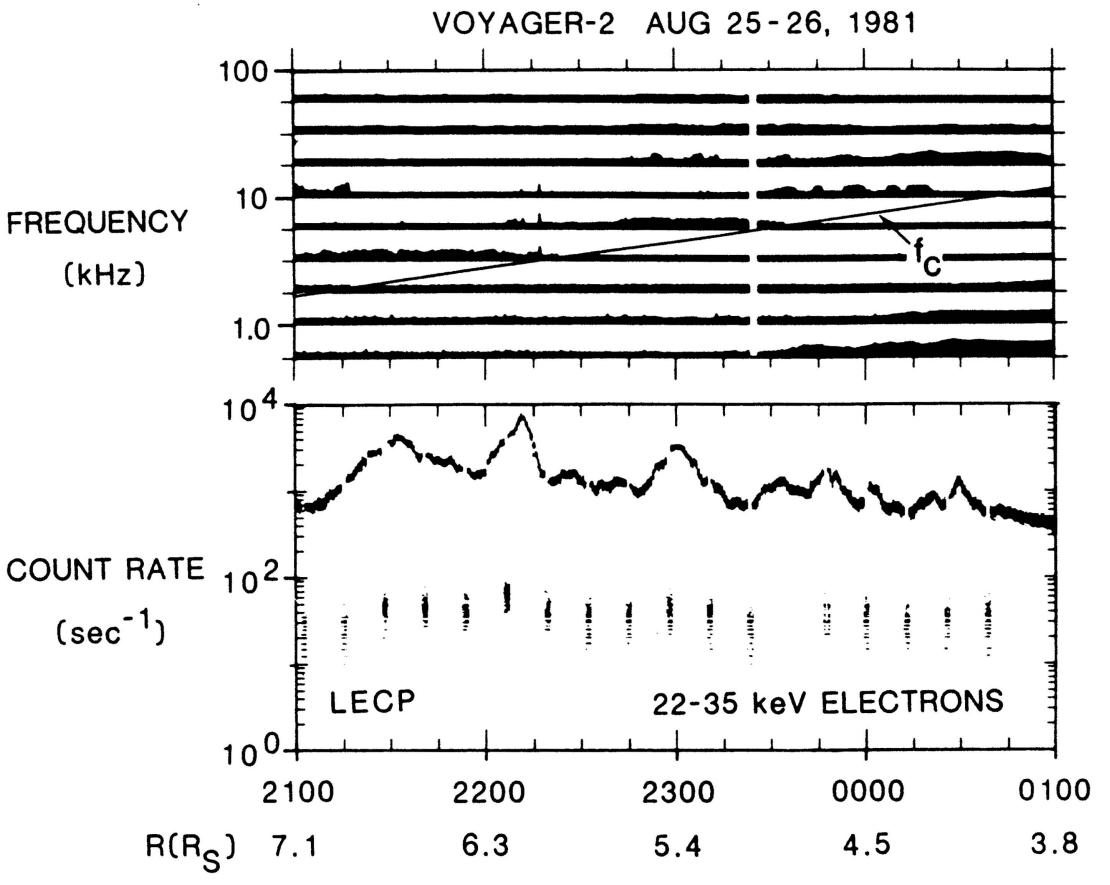

Fig. 18. Simultaneous plasma wave and LECP data of Voyager 2 showing evidence for several keV electron fluxes which may be interacting with the $(n + 1/2)f_c$ emissions seen in the upper panel.

keV electrons could be the high-energy end of the spectrum of electrons responsible for driving the electron cyclotron harmonic instability. Since all occurrences of the $(n + 1/2)f_g$ emissions are not accompanied by variable rates in the 22–35 keV channel, they conjectured that lower energy electrons, below the LECP instrument threshold and above the plasma science instrument (PLS) threshold, might drive the waves.

Barbosa and Kurth (1980) studied the quantitative relation between suprathermal electrons and electron cyclotron harmonic emissions in order to identify the electrons responsible for driving such waves. One important result of their analysis is that large convective growth rates in the lower portion of a harmonic band, as for the case of the Saturnian 3/2 band, can be the result of resonant electrons having a velocity V_r only a few times the thermal speed of the cool background. The lower panel of Fig. 19 contains a 4-second average wave spectrum from Voyager 2 outbound (0736, 26 August 1981). The frequency scale in Fig. 19 (upper panel) is the normalized frequency $\bar{\omega} = f/f_g$; it should be noted that the emission is confined to the very bottom of the first harmonic band.

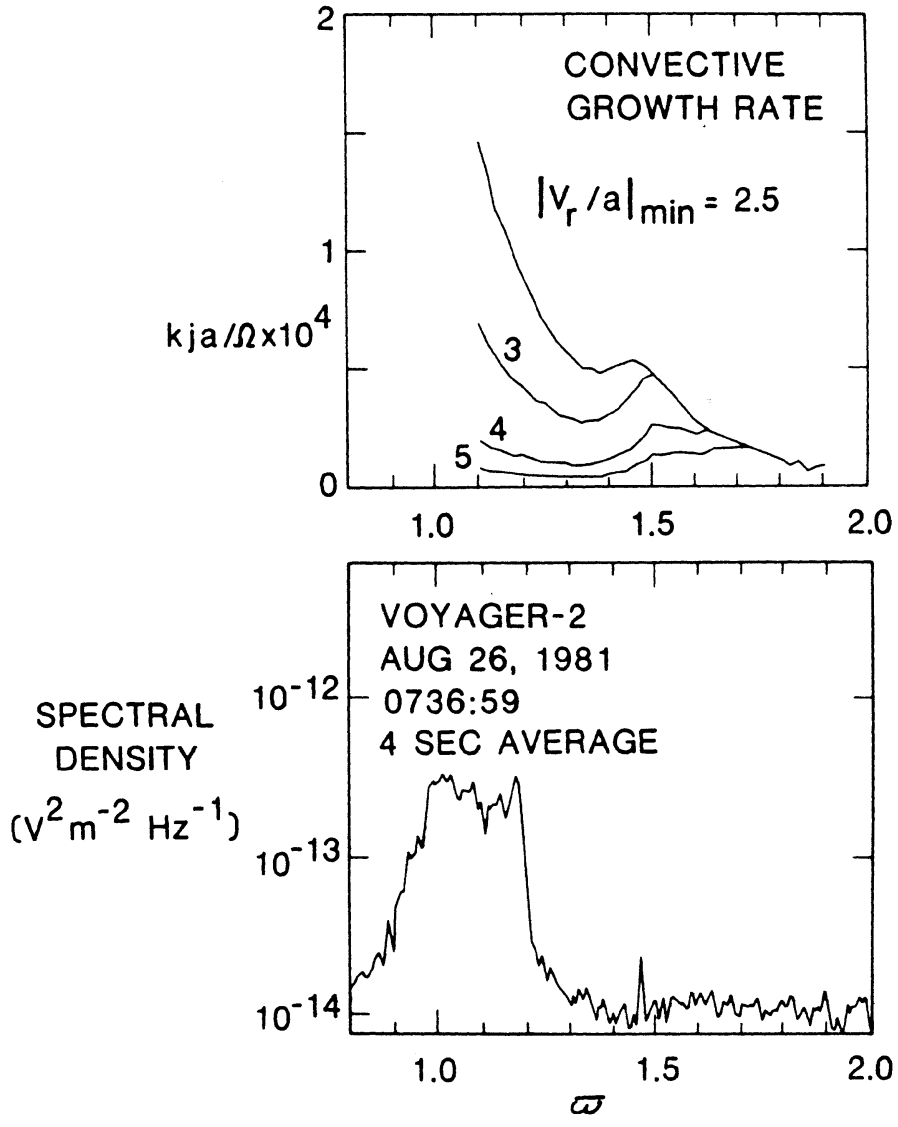

Fig. 19. A comparison of the spectrum of a typical 3/2 band observed at Saturn (lower panel) with convective growth rates (upper panel). The Saturn emission is confined to the lower portion of the band between f_c and $2f_c$, $\tilde{\omega} \lesssim 1.3$. This implies that $|V_r/a|_{min}$ is small ($\lesssim 3$).

In the right-hand panel of Fig. 19 the convective growth rates are shown for $|V_r/a|_{min} = 2.5, 3, 4$, and 5 (here a is the thermal speed). Kurth et al. (1983) used $Tj_\perp = 1.1 \times 10^5\,\mathrm{cm^{-2}\,s^{-1}\,sr^{-1}}$, $n_c = 1.6\,\mathrm{cm^{-3}}$, and $T_c = 8$ eV. They also found that smaller values of $|V_r/a|_{min}$ yield growth rate curves nearly similar to the measured wave spectrum, although they caution the reader that spectral density cannot be directly related to growth rate. However, the comparison between theory and experiment did suggest $T_R = 9\,T_c$, where T_R and T_c refer to temperatures of resonant and cool electrons, respectively.

For the Voyager 2 inbound measurements near 2300 UT on 25 August, $T_c \approx 8$ eV implying $T_R \sim 70$ eV. Kurth et al. noted that the actual value of T_R/T_c is not well specified, but concluded that T_R is on the order of 100 eV and not

several keV as might be suggested by the enhanced fluxes of 22 to 35 keV electrons evident in Fig. 18. Thus, it seems that the electrons observed by LECP are not driving the electron cyclotron instability, although those electrons may very well be scattered by or perhaps even stochastically accelerated by the electrostatic waves. This conclusion is also supported by the theoretical analyses of Ashour-Abdalla and Kennel (1978), Hubbard and Birmingham (1978), and Hubbard et al. (1979) who calculated that values of $|V_r/a| \approx 3$ were suitable for optimal growth of 3/2 emissions at Earth.

Nevertheless, the plasma probe measurements did provide conclusive simultaneous evidence of a 100 to 200 eV suprathermal electron component with a density of $\sim 0.16\ \mathrm{cm}^{-3}$, so we must turn to theoretical arguments. For Jupiter, Barbosa and Kurth (1980) derived a quantity $Tj_{\perp}^{*}(T)$ defined as the critical flux of resonant electrons able to produce 10 e foldings in amplitude of electron cyclotron waves in the Jovian magnetosphere:

$$Tj_{\perp}^{*}(T) = 23\left(\frac{0.1}{\delta\bar{\omega}}\right) pR^2\bar{\omega}\ (\mathrm{cm}^2\ \mathrm{s\ sr})^{-1}. \tag{11}$$

Here, T is the electron temperature in eV, $\bar{\omega}$ is the wave frequency normalized to f_g ($\bar{\omega} = f/f_g$), p is the pressure due to cool background electrons ($p = n_cT_c$) in units of eV cm^{-3}, and R is in planetary radii. Equation (11) can be modified for use at Saturn as follows:

$$Tj_{\perp}^{*}(T = T_R) = 23\left(\frac{0.1}{\delta\bar{\omega}}\right)\left(\frac{4.2G}{B_s}\right)\left(\frac{7.13 \times 10^4\ \mathrm{km}}{\mathrm{R_S}}\right)\left(\frac{T/T_c}{9}\right)^2 pR\bar{\omega}. \tag{12}$$

B_s is the surface field magnitude at Saturn, 0.21 G and $\mathrm{R_S}$ is 6×10^4 km. Following Barbosa and Kurth, Kurth et al. (1983) chose $\bar{\omega} = 1.3$ and $\delta\bar{\omega} = 0.25$ based on the measured frequencies and bandwidths of the Saturn emissions.

Kurth et al. (1983) evaluated Eq. (12) using wave and particle measurements for Voyager 2 inbound at 2324, 25 August ($R = 5\ \mathrm{R_S}$); they found $Tj_{\perp}^{*} = 1.1 \times 10^5\ (\mathrm{cm}^2\ \mathrm{s\ sr})^{-1}$. The critical flux of resonant electrons from Eq. (12) was compared to the measured flux. Given $T_H = 100$ eV and $n_H = 0.16\ \mathrm{cm}^{-3}$, the measured flux of hot electrons is $7.6 \times 10^6\ (\mathrm{cm}^2\ \mathrm{s\ sr})^{-1}$ or 76 times greater than the critical flux. This result seems satisfactory, since fluxes substantially larger than $Tj_{\perp}^{*}$ are probably required, because at this time Voyager was 28° above the equator, where conditions for wave growth would not be optimum. The preliminary conclusions reported by Kurth et al. (1983) suggest that at Saturn the suprathermal electrons detected by the plasma probe generate the electron cyclotron harmonic waves, and that these waves in turn may cause diffusion or even acceleration of electrons with energies in the range of tens of kilovolts.

VII. DISCUSSION

In order to evaluate the dynamics of Saturn's magnetosphere from the limited set of observations now available, certain ground rules must be adopted. In particular, when we use combined data from Pioneer 11, Voyager 1, and Voyager 2, we tacitly assume that the overall system is basically constant in time and that all important changes in measurements are associated with the different traversals of distinct spatial features. However, in terms of energetic particle measurements, it has been noted that Pioneer 11 encountered Saturn in an extremely disturbed state during one of the largest solar particle events of the current solar cycle (Simpson et al. 1980*b*). In contrast, both Voyager encounters in November 1980 and August 1981 occurred at times when the interplanetary medium in the vicinity of Saturn was relatively quiet for higher energy particles. Thus, the magnetosphere of Saturn was observed by Voyager in a more or less quiescent state, although significant temporal variations did occur between encounters and while the two encounters were in progress (Ness et al. 1981; Krimigis et al. 1982*a*; Maclennan et al. 1983).

In terms of phenomena of low-energy plasma physics, we note that the Saturn flyby of Voyager 2 was still unusual because at that time the solar wind pressure was low and variable, and the Saturn system was nearly lined up with Jupiter's extended magnetic tail. Scarf et al. (1983) presented evidence that Voyager was near the Jovian tail *after* the Saturn encounter. This suggested that Saturn may have been immersed in Jupiter's tail during a portion of the Voyager 2 encounter, as originally conjectured by Scarf (1979); Desch (1983) recently discussed changes in the radio emission pattern that strongly support this concept.

Despite these concerns about temporal variations, the measurements from the three spacecraft do appear to be reasonably consistent in terms of particle and field distributions in the inner magnetosphere. Although the Pioneer and Voyager trajectories and measurement capabilities did not overlap completely, there is no compelling reason to believe that the data sets are incompatible. Thus, one might expect that enough information was gathered during the three encounters to provide the foundation for constructing a dynamic model, based on synthesis of all the observations.

In fact, the data show that the Saturn system is extremely complex and that there are still a large number of fundamental uncertainties associated with interpretations of the spacecraft measurements. The rings and the many icy satellites in the inner magnetosphere are potential sources of plasma, and they also act as sinks. It has been conjectured that dust particles from satellites such as Enceladus cause plasma losses and even plasma cooling. The apparent modulation of radio emissions associated with the orbital phase of Dione (Gurnett et al. 1981*a*; Warwick et al. 1981; Kurth et al. 1981*b*) could even mean that this satellite was venting gases during the Voyager 1 encounter. Be-

cause the system is so complex, questions related to sources and sinks of plasma and suprathermal particles are largely unanswered; it is possible that charged particles observed in the inner magnetosphere originate in the solar wind, in Saturn's atmosphere, in the main ring system, the icy satellites, the atmosphere of Titan, or even in the tenuous E and G Rings. Since the spacecraft measurements of plasma composition are generally not precise enough to identify sources and sinks, it is likely that many significant questions involving magnetospheric dynamics will remain unanswered until a follow-up mission to the Saturn system is carried out.